Lepton flavor violating Higgs boson decays from massive seesaw neutrinos

Ernesto Arganda,* Ana M. Curiel,† and María J. Herrero‡
Departamento de Física Teórica, Universidad Autónoma de Madrid, Spain

David Temes§
Laboratoire de Physique Théorique, LAPTH, France‖
(Received 3 November 2004; published 15 February 2005)

Lepton flavor violating Higgs boson decays are studied within the context of seesaw models with Majorana massive neutrinos. Two models are considered: the SM-seesaw, with the standard model particle content plus three right-handed neutrinos, and the MSSM-seesaw, with the minimal supersymmetric standard model particle content plus three right-handed neutrinos and their supersymmetric partners. The widths for these decays are derived from a full one-loop diagrammatic computation in both models, and they are analyzed numerically in terms of the seesaw parameters, namely, the Dirac and Majorana mass matrices. Several possible scenarios for these mass matrices that are compatible with neutrino data are considered. In the SM-seesaw case, very small branching ratios are found for all studied scenarios. These ratios are explained as a consequence of the decoupling behavior of the heavy right-handed neutrinos. In contrast, in the MSSM-seesaw case, sizable branching ratios are found for some of the leptonic flavor violating decays of the MSSM neutral Higgs bosons and for some choices of the seesaw matrices and MSSM parameters. The relevance of the two competing sources of lepton flavor changing interactions in the MSSM-seesaw case is also discussed. The nondecoupling behavior of the supersymmetric particles contributing in the loop diagrams is finally shown.

DOI: 10.1103/PhysRevD.71.035011 PACS numbers: 14.80.Cp, 12.15.Lk, 12.60.Jv, 14.60.Pq

I. INTRODUCTION

The present strong evidence for lepton flavor changing neutrino oscillations [1] in solar and atmospheric neutrino data, as well as in the KamLAND reactor experiment, implies the existence of nonzero masses for the light neutrinos and provides the first experimental clue for physics beyond the standard model (SM). The experimentally suggested smallness of the neutrino masses can be explained in a very simple and elegant way by the seesaw mechanism of neutrino mass generation [2]. This mechanism requires the introduction of heavy right-handed (RH) Majorana neutrinos which are singlet under the SM gauge symmetry group and whose Majorana masses m_{M_i} can therefore be much higher than the SM particle masses. In this context, the smallness of the light left-handed (LH) neutrino masses appears naturally due to the induced large suppression by the ratio of the two very distant mass scales that are involved in the seesaw mass matrices, the Majorana matrix m_M and the Dirac matrix m_D. The latter is generated after electroweak symmetry breaking by $m_D = Y_\nu \langle H \rangle$, where Y_ν is the Yukawa matrix for couplings between the RH and LH neutrinos and $\langle H \rangle = v = 174$ GeV is the SM Higgs boson vacuum expectation value. For the one generation case, and assuming a Yukawa coupling of order one, the suggested small neutrino mass value signals towards a new physics mass scale of the order of $m_M \sim 10^{14}$ GeV, but the pattern and size of the seesaw mass parameters can vary much in respect to this in the most general case of three generations.

Another appealing feature of the seesaw models is that the RH Majorana neutrinos can successfully generate, through their *CP*-violating decays and via leptogenesis, the observed baryon asymmetry of the Universe. There is, however, one negative aspect in the standard version of the seesaw models. It is that the presence of the two distant mass scales can lead to a severe hierarchy problem, and this requires the introduction of supersymmetry (SUSY) to be solved. In the SUSY-seesaw models, the hierarchy between m_M and the electroweak scale is stabilized by the new contributions of the SUSY partners of the RH and LH neutrinos. Thus, the SUSY-seesaw models, and particularly the simplest version given by the minimal supersymmetric standard model (MSSM), are becoming more popular.

One of the most interesting features of the SUSY-seesaw models is the associated rich phenomenology due to the occurrence of lepton flavor violating (LFV) processes. Whereas in the standard (non-SUSY) seesaw models the ratios of LFV processes are small due to the smallness of the light neutrino masses, in the SUSY-seesaw models these can be large due to an important additional source of lepton flavor mixing in the soft-SUSY-breaking terms. Even in the scenarios with universal soft-SUSY-breaking parameters at the large energy scale associated to the SUSY-breaking M_X (which could be the Planck mass, the SUSY-grand unified theory mass or something else, but

*Electronic address: ernesto.arganda@uam.es
†Electronic address: ana.curiel@uam.es
‡Electronic address: maria.herrero@uam.es
§Electronic address: temes@lapp.in2p3.fr
‖UMR 5108 du CNRS, associée à l'Université de Savoie.

always well above m_M), the running from this scale down to m_M induces, via the neutrino Yukawa couplings Y_ν, large lepton flavor mixing in the slepton soft masses and provides the so-called slepton-lepton misalignment, which in turn generates nondiagonal lepton flavor interactions. These interactions can induce sizable ratios in several LFV processes with SM charged leptons in the external legs, which are actually being tested experimentally with high precision and therefore provide a very interesting window to look for indirect SUSY signals.

In addition to the previously mentioned radiatively induced LFV effect, there is another source of radiative LFV effects in the MSSM-seesaw, which is generated from the neutrino sector mixing. Namely, the off-diagonal entries of the Maki-Nakagawa-Sakata (MNS) matrix $U_{\rm MNS}$ [3] produce lepton flavor nondiagonal interactions involving neutrinos which could also generate, via loops, important contributions to the LFV processes with SM leptons in the external legs. In the MSSM-seesaw, these LFV effects from neutrino mixing could indeed compete in some processes with the other source from slepton-lepton misalignment. This competitivity of the two flavor changing sources has indeed been noticed previously in the squark sector, concretely in the SUSY-electroweak one-loop contributions to flavor changing Higgs boson decays, $h^0 \to \bar{b}s, \bar{s}b$ [4]. Interestingly, the lepton sector could manifest more evidently these competing effects than the quark sector, since the MNS matrix being preferred by neutrino data is clearly nondiagonal, whereas the Cabibbo-Kobayashi-Maskawa matrix is close to the identity matrix.

Among the various LFV processes that have been considered in the literature, the most fruitful ones are the radiative $\mu \to e\gamma$, $\tau \to \mu\gamma$, and $\tau \to e\gamma$ decays [5–8], since their branching ratios are tested with high precision [9–11]. These usually provide the most restrictive experimental bounds on the MSSM-seesaw parameters. Other interesting LFV decays include τ rare decays, Z boson decays $Z \to l_k \bar{l}_m$, and Higgs boson decays $H \to l_k \bar{l}_m$, with $k \neq m$.

We are interested here in the LFV Higgs boson decays (LFVHD), $H \to \tau\bar{\mu}, \tau\bar{e}, \mu\bar{e}$, and the branching ratios that can be generated in the context of the seesaw models with parameters being compatible with the neutrino data and the most relevant data of τ and μ radiative decays. In this work we consider both versions of the seesaw mechanism for neutrino mass generation: the SM-seesaw and the MSSM-seesaw. In the first one, the SM particle content is enlarged by three singlet RH Majorana neutrinos, and in the second one, the MSSM particle content is enlarged by three singlet RH Majorana neutrinos and their corresponding SUSY partners. We present here a complete one-loop computation of the LFVHD widths in both seesaw scenarios and analyze the size of the associated branching ratios in terms of the seesaw parameters. In order to make contact between the seesaw mass matrices and the experimental neutrino data, we use the general parametrization introduced in Ref. [6], where the Yukawa neutrino couplings, and therefore m_D, are expressed in terms of the three physical light neutrino masses m_{ν_i}, the three physical heavy neutrino masses m_{N_i}, the $U_{\rm MNS}$ matrix, and a general complex 3×3 orthogonal matrix R.

The LFVHD within the SM-seesaw was studied some time ago in Ref. [12]. There it was considered a very specific seesaw scenario where all the light neutrinos were exactly massless at tree level [13] and the Dirac mass was taken very large. The conclusion was that branching ratios for $H_{\rm SM} \to \tau\bar{\mu}$ decays as large as 10^{-4}–10^{-5} can be achieved for $m_{H_{\rm SM}} \leq 140$ GeV. Besides, these ratios were found to grow with the heavy neutrino masses, and this growth suggested a nondecoupling behavior of the heavy neutrinos. The crucial assumption for that behavior was to take very large m_D values, which implied very strong neutrino Yukawa couplings. Here we have recalculated the LFVHD rates in the complete one-loop diagrammatic approach and updated the numerical estimates in light of the recent neutrino data, by fixing the input parameters m_{ν_i} and $U_{\rm MNS}$ to their data preferred values. We then make our estimates for specific choices of the input unknown parameters m_{N_i} and R and pay special attention to those which generate successful baryon asymmetry. For all the studied cases we find ratios that are many orders of magnitude smaller than in Ref. [12]. The reason for these small ratios is because the heavy RH neutrinos do indeed decouple in our SM-seesaw scenario and our assumptions for the seesaw parameters do not imply large m_D values. For completeness, we also include in this part an estimate of the LFVHD rates in the case of Dirac massive neutrinos and compare them with the previous estimate of Ref. [14].

The second part of this work concerns the evaluation of the LFVHD ratios in the context of the MSSM-seesaw. Concretely, $h^0, H^0, A^0 \to l_k \bar{l}_m$, with $k \neq m$. The subject of LFVHD being generated from loops of SUSY particles has been considered previously in Refs. [14,15]. In Ref. [14] it was analyzed a specific SUSY-SU(5) scenario where the slepton-lepton misalignment was generated exclusively from the running of the trilinear A terms. On the other hand, the computation of Ref. [15] was not in the context of the MSSM-seesaw but in a more generic scenario for slepton-lepton misalignment. Besides, in Ref. [15], the effective Lagrangian approach that is valid for large $\tan\beta$ values and large SUSY mass values is used. We present here instead a complete one-loop computation in the MSSM-seesaw context and do not rely on any of the above approximations. We include in the computation both sources of lepton flavor violating interactions, the slepton-lepton misalignment, and the neutrino mixing via $U_{\rm MNS}$. The slepton-lepton misalignment is generated, as is usual in the seesaw models, by the renormalization group running of the slepton soft parameters from the high en-

ergies M_X down to m_M. The diagonalization of the generated slepton mass matrix is then performed. That is, we do not rely on either the mass insertion approximation or the large $\tan\beta$ effective Lagrangian approach and, therefore, our results are valid for all $\tan\beta$ values and all soft-SUSY-breaking mass values. We will explore the size of the branching ratios for the Higgs decays as a function of the relevant MSSM parameters, which within the context of minimal supergravity (mSUGRA) are the universal soft masses M_0, $M_{1/2}$, and $\tan\beta$, and of the relevant seesaw parameters, which are m_{N_i} and the R matrix. We will analyze in parallel the branching ratios for the $l_j \to l_i\gamma$ decays as a function of the same parameters. The requirement of compatibility with the present data on $l_j \to l_i\gamma$ decays, mainly $\mu \to e\gamma$ and $\tau \to \mu\gamma$, will provide us with the maximum allowed ratios for the Higgs decays. We will also study the behavior of the LFVHD widths in the limit of very heavy SUSY masses and will find that the sleptons, sneutrinos, charginos, and neutralinos do not decouple in this observable. For large SUSY masses, large $\tan\beta$, and particular choices of the seesaw parameters, we will find agreement with the numerical results of Ref. [15].

The paper is organized as follows. Section II contains a short summary of the mass parameters and mixings in the neutrino sector of the seesaw models. The relation between these parameters and the experimental neutrino masses and mixings is also included. Section III is devoted to the computation and analysis of the LFVHD rates in the context of the SM-seesaw. The decoupling behavior of the heavy neutrinos is also studied in this section. Section IV starts by presenting the two sources of LFV interactions in the context of the MSSM-seesaw. Next the computation and analysis of the LFVHD rates within that context is included. The nondecoupling behavior of the SUSY particles in the LFVHD widths is studied at the end of this section. Section V is devoted to the conclusions.

II. NEUTRINO MASSES AND MIXINGS IN THE SEESAW MODELS

In this section and in order to fix our notation, we briefly review the mass parameters and mixings in the neutrino sector of the seesaw models and relate them to the physical light neutrino masses and neutrino mixing angles which are extracted from neutrino data. We follow closely here and in the next sections the notation of Refs. [12,13] for SM-seesaw and Ref. [6] for SUSY seesaw and for the connection with neutrino data.

We start with the Yukawa sector of the SM-seesaw that contains the three LH SM neutrinos $\nu^o_{L,i}$ and three extra RH massive neutrinos $\nu^o_{R,i}$, whose Yukawa interactions provide, after spontaneous electroweak symmetry breaking, together with the right-handed neutrino masses, the following mass Lagrangian containing the Dirac and Majorana mass terms:

$$-L^{\nu}_{\text{mass}} = \frac{1}{2}[\overline{\nu}^0_L, (\overline{\nu}^0_R)^C]M^{\nu}\begin{bmatrix} (\nu^0_L)^C \\ \nu^0_R \end{bmatrix} + \text{H.c.}, \tag{1}$$

where

$$M^{\nu} = \begin{pmatrix} 0 & m_D \\ m_D^T & m_M \end{pmatrix}. \tag{2}$$

Here m_D is the 3×3 Dirac mass matrix that is related to the 3×3 Yukawa coupling matrix Y_ν and the SM Higgs vacuum expectation value, $\langle H\rangle = v = 174$ GeV, by $m_D = Y_\nu\langle H\rangle$, and m_M is the 3×3 Majorana mass matrix for the RH massive neutrinos that is real, nonsingular, and symmetric.

The mass matrix M^ν is a 6×6 complex symmetric matrix that can be diagonalized by a 6×6 unitary matrix U^ν in the following way:

$$U^{\nu T}M^{\nu}U^{\nu} = \hat{M}^{\nu} = \text{diag}(m_{\nu_1}, m_{\nu_2}, m_{\nu_3}, m_{N_1}, m_{N_2}, m_{N_3}). \tag{3}$$

This gives three light Majorana neutrino mass eigenstates ν_i, with masses m_{ν_i} $(i = 1, 2, 3)$, and three heavy ones N_i, with masses m_{N_i} $(i = 1, 2, 3)$, which are related to the weak eigenstates via

$$\begin{bmatrix} \nu^0_L \\ (\nu^0_R)^C \end{bmatrix} = U^{\nu *}\begin{pmatrix} \nu_L \\ N_L \end{pmatrix} \quad \text{and} \quad \begin{bmatrix} (\nu^0_L)^C \\ \nu^0_R \end{bmatrix} = U^{\nu}\begin{pmatrix} \nu_R \\ N_R \end{pmatrix}. \tag{4}$$

The seesaw mechanism for neutrino mass generation assumes a large separation between the two mass scales involved in m_D and m_M matrices. More specifically, we shall assume here that all matrix elements of m_D are much smaller than those of m_M, $m_D \ll m_M$, and we will perform an analytical expansion of all relevant interaction parameters and observables in power series of a matrix defined as

$$\xi \equiv m_D m_M^{-1}. \tag{5}$$

In particular, the previous diagonalization of the mass matrix M^ν can be solved in power series of ξ [16]. For simplicity, we choose to work here and in the rest of this paper in a flavor basis where the RH Majorana mass matrix m_M and the charged lepton mass matrix M^l are flavor diagonal. This means that all flavor mixing of the light sector is included in the mixing matrix U_{MNS}. By working to the lowest orders of these power series expansions one finds, in the flavor basis, the following neutrino 3×3 matrices:

$$\begin{aligned} m_\nu &= -m_D\xi^T + \mathcal{O}(m_D\xi^3) \simeq -m_D m_M^{-1} m_D^T, \\ m_N &= m_M + \mathcal{O}(m_D\xi) \simeq m_M. \end{aligned} \tag{6}$$

Here m_N is already diagonal, but m_ν is not yet diagonal. The rotation from this flavor basis to the mass eigenstate

basis is finally given by the MNS unitary matrix $U_{\rm MNS}$. Thus,

$$\begin{aligned} m_\nu^{\rm diag} &= U_{\rm MNS}^T m_\nu U_{\rm MNS} = {\rm diag}(m_{\nu_1}, m_{\nu_2}, m_{\nu_3}), \\ m_N^{\rm diag} &= m_N = {\rm diag}(m_{N_1}, m_{N_2}, m_{N_3}), \end{aligned} \tag{7}$$

and the diagonalization of M^ν in Eqs. (2) and (3) can be performed by the following unitary 6×6 matrix:

$$U^\nu = \begin{bmatrix} (1 - \frac{1}{2}\xi^*\xi^T)U_{\rm MNS} & \xi^*(1 - \frac{1}{2}\xi^T\xi^*) \\ -\xi^T(1 - \frac{1}{2}\xi^*\xi^T)U_{\rm MNS} & (1 - \frac{1}{2}\xi^T\xi^*) \end{bmatrix} + \mathcal{O}(\xi^4). \tag{8}$$

As for the $U_{\rm MNS}$ matrix, we use the standard parametrization given by

$$U_{\rm MNS} = \begin{pmatrix} c_{12}c_{13} & s_{12}c_{13} & s_{13}e^{-i\delta} \\ -s_{12}c_{23} - c_{12}s_{23}s_{13}e^{i\delta} & c_{12}c_{23} - s_{12}s_{23}s_{13}e^{i\delta} & s_{23}c_{13} \\ s_{12}s_{23} - c_{12}c_{23}s_{13}e^{i\delta} & -c_{12}s_{23} - s_{12}c_{23}s_{13}e^{i\delta} & c_{23}c_{13} \end{pmatrix} {\rm diag}(1, e^{i\alpha}, e^{i\beta}), \tag{9}$$

where $c_{ij} \equiv \cos\theta_{ij}$ and $s_{ij} \equiv \sin\theta_{ij}$.

Finally, in order to make contact with the experimental data, we use the method proposed in Ref. [6]. It provides a simple way to reconstruct the Dirac mass matrix by starting with the physical light and heavy neutrino masses, the $U_{\rm MNS}$ matrix, and a general complex and orthogonal matrix R. With our signs and matrix conventions this relation can be written as

$$m_D^T = i m_N^{{\rm diag}\,1/2} R m_\nu^{{\rm diag}\,1/2} U_{\rm MNS}^+, \tag{10}$$

where $R^T R = 1$. Thus, instead of proposing directly possible textures for m_D, one proposes possible values for $m_{N_1}, m_{N_2}, m_{N_3}$, and R and sets $m_{\nu_1}, m_{\nu_2}, m_{\nu_3}$, and $U_{\rm MNS}$ to their suggested values from the experimental data. Notice that any hypothesis for R different from the unit matrix will lead to an additional lepton flavor mixing between the LH and RH neutrino sectors. Notice also that the previous relation holds at the energy scale m_M and to use it properly one must use the renormalization group equations (RGE) to run the input experimental data $m_\nu^{\rm diag}$ and $U_{\rm MNS}$ from the low energies m_W up to m_M. We have computed here these running effects by solving the RGE in the one-loop approximation [17], and we have considered the corresponding radiatively corrected neutrino masses and $U_{\rm MNS}$ matrix elements in our computation of the LFV rates.

For the numerical estimates in this paper, we will consider the following two plausible scenarios, at the low energies, being compatible with data:

Scenario A quasidegenerate light and degenerate heavy neutrinos,

$$\begin{aligned} &m_{\nu_1} = 0.2 \text{ eV}, \qquad m_{\nu_2} = m_{\nu_1} + \frac{\Delta m^2_{\rm sol}}{2m_{\nu_1}}, \\ &m_{\nu_3} = m_{\nu_1} + \frac{\Delta m^2_{\rm atm}}{2m_{\nu_1}}, \\ &m_{N_1} = m_{N_2} = m_{N_3} = m_N. \end{aligned} \tag{11}$$

Scenario B hierarchical light and hierarchical heavy neutrinos,

$$\begin{aligned} &m_{\nu_1} \simeq 0 \text{ eV}, \qquad m_{\nu_2} = \sqrt{\Delta m^2_{\rm sol}}, \\ &m_{\nu_3} = \sqrt{\Delta m^2_{\rm atm}}, \qquad m_{N_1} \le m_{N_2} < m_{N_3}. \end{aligned} \tag{12}$$

In the two above scenarios, we will fix the input low energy data to the following values: $\sqrt{\Delta m^2_{\rm sol}} = 0.008$ eV, $\sqrt{\Delta m^2_{\rm atm}} = 0.05$ eV, $\theta_{12} = \theta_{\rm sol} = 30^\circ$, $\theta_{23} = \theta_{\rm atm} = 45^\circ$, $\theta_{13} = 0^\circ$, and $\delta = \alpha = \beta = 0$ (see, for instance, Ref. [18]).

Regarding the matrix R, we will consider correspondingly one of the following three cases:

Case 0

$$R = R_0 = 1. \tag{13}$$

This is a reference case which is chosen here just because it is the simplest possibility.

Case 1

$$R = R_1 = \begin{pmatrix} c_2c_3 & -c_1s_3 - s_1s_2c_3 & s_1s_3 - c_1s_2c_3 \\ c_2s_3 & c_1c_3 - s_1s_2s_3 & -s_1c_3 - c_1s_2s_3 \\ s_2 & s_1c_2 & c_1c_2 \end{pmatrix}, \tag{14}$$

where $c_i \equiv \cos\theta_i$, $s_i \equiv \sin\theta_i$, and θ_1, θ_2, and θ_3 are arbitrary complex angles. This parametrization was proposed in Ref. [6] for the study of $\mu \to e\gamma$ decays. It has also been considered in Ref. [7] with specific values for the θ_i angles to study the implications for baryogenesis in the case of hierarchical neutrinos.

Case 2

$$R = R_2 = e^{iA} O, \tag{15}$$

with $O = 1$ and

$$A = \begin{pmatrix} 0 & a & b \\ -a & 0 & c \\ -b & -c & 0 \end{pmatrix}. \tag{16}$$

Here a, b, and c are three real parameters that are constrained by perturbativity of the Yukawa couplings. In particular, for $a = b = c \equiv k$ and $m_{\nu_{1,2,3}} \simeq 0.2$ eV, it leads to $k < (1.4, 0.9, 0.3)$ for $m_{N_{1,2,3}} \simeq (10^{10}, 10^{12}, 10^{14})$ GeV, respectively. This choice has been proven in Ref. [8] to provide successful baryon asymmetry via leptogenesis for the case of quasidegenerate neutrinos.

All that has been summarized in this section applies to the MSSM-seesaw model as well. The only difference is that, in this case, m_D is related to one of the two Higgs vacuum expectation values by $m_D = Y_\nu \langle H_2 \rangle$, where $\langle H_2 \rangle = v_2 = v \sin\beta$.

III. LEPTON FLAVOR VIOLATING HIGGS DECAYS IN THE SM SEESAW

In this section, we compute and analyze the LFVHD widths, $\Gamma(H \to l_k \bar{l}_m)$ with $k \neq m$, within the context of the SM-seesaw with three RH neutrinos which has been shortly reviewed in the previous section. The branching ratios for these decays were studied some time ago in Ref. [12] in a particular scenario of the SM-seesaw where all the light neutrino masses were exactly zero at the tree level and the Dirac mass was taken very large. The small masses for the light neutrinos were then generated by the one-loop electroweak radiative corrections [13]. Besides, the numerical results of Ref. [12] for the case of three generations were obtained under particular approximations for the evaluation of the one-loop diagrams as, for instance, $m_{l_1} = 0$, $m_{l_2}^2/m_W^2 \ll 1$, $m_H^2/4m_W^2 \ll 1$, the latter being nowadays clearly not a very good approximation given the present lower bound on m_H from LEP of about 115 GeV. Here we have recomputed these LFVHD widths for all the channels and we have included all contributing one-loop diagrams without assuming any approximation. One of the main points of our analysis is the update of the numerical results by taking into account the present experimental neutrino data. In addition, we will reanalyze the behavior of these partial widths with the large heavy neutrino masses. In contrast to Ref. [12], where the important enhancement of the widths found with m_{N_i} suggested a nondecoupling behavior of the heavy neutrinos, we will find instead a clear decoupling behavior. The main difference between Ref. [12] and us is the assumption on m_D, which in their work was taken very large (therefore, leading to strong neutrino Yukawa couplings), whereas in our case the assumptions for the input m_{N_i} and R do not lead to large m_D.

We start by writing down the interactions that are relevant for the computation of the LFVHD widths to one loop and in the mass eigenstate basis. Denoting the Majorana neutrino mass eigenstates collectively by n_i (i.e., $n_i \equiv \nu_i$ for $i = 1, 2, 3$ and $n_i = N_{i-3}$ for $i = 4, 5, 6$), the relevant interactions between n_i and $W^\pm$, H, and the Goldstone bosons $G^\pm$ can be written, respectively, as follows:

$$\begin{aligned} \mathcal{L}_{\rm int}^{W^\pm} &= \frac{-g}{\sqrt{2}} W^{\mu -} \bar{l}_i B_{l_i n_j} \gamma_\mu P_L n_j + \text{H.c.}, \\ \mathcal{L}_{\rm int}^{H} &= \frac{-g}{4 m_W} H \bar{n}_i [(m_{n_i} + m_{n_j}) \text{Re}(C_{n_i n_j}) \\ &\quad + i \gamma_5 (m_{n_j} - m_{n_i}) \text{Im}(C_{n_i n_j})] n_j, \\ \mathcal{L}_{\rm int}^{G^\pm} &= \frac{-g}{\sqrt{2} m_W} G^{\mu -} [\bar{l}_i B_{l_i n_j} (m_{l_i} P_L - m_{n_j} P_R) n_j] + \text{H.c.}, \end{aligned} \tag{17}$$

where the coupling factors $B_{l_i n_j}$ ($i = 1, 2, 3$, $j = 1, \ldots, 6$) and $C_{n_i n_j}$ ($i, j = 1, \ldots, 6$) are defined in terms of the U^ν matrix of Eq. (3) by

$$B_{l_i n_j} = U^{\nu *}_{ij}, \tag{18}$$

$$C_{n_i n_j} = \sum_{k=1}^{3} U^\nu_{ki} U^{\nu *}_{kj}. \tag{19}$$

Notice that our particular choice of diagonal charged leptons in the flavor basis is equivalent to assuming a V matrix in Ref. [12] equal to the identity matrix. The expansions of these coupling matrices in power series of the ξ matrix can be easily derived from the expansion of U^ν in Eq. (8). For brevity, we omit here the indices and use a self-explanatory short notation. They are given by

$$B_{ln} = (B_{l\nu}, B_{lN}), \tag{20}$$

$$C_{nn} = \begin{pmatrix} C_{\nu\nu} & C_{\nu N} \\ C_{N\nu} & C_{NN} \end{pmatrix}, \tag{21}$$

where

$$\begin{aligned} B_{l\nu} &= (1 - \tfrac{1}{2} \xi \xi^+) U^*_{\rm MNS} + \mathcal{O}(\xi^4), \\ B_{lN} &= \xi (1 - \tfrac{1}{2} \xi^+ \xi) + \mathcal{O}(\xi^5), \\ C_{\nu\nu} &= U^T_{\rm MNS} (1 - \xi \xi^+) U^*_{\rm MNS} + \mathcal{O}(\xi^4), \\ C_{\nu N} &= C^+_{N\nu} = U^T_{\rm MNS} \xi (1 - \xi^+ \xi) + \mathcal{O}(\xi^5), \\ C_{NN} &= \xi^+ \xi + \mathcal{O}(\xi^4). \end{aligned} \tag{22}$$

After the computation of the ten contributing one-loop diagrams, drawn in Fig. 1, we find the analytical results presented in Appendix A which have been written in terms of the standard one-loop integrals, $C_0, B_0, C_{12}, \ldots$, etc., whose definitions can be found, for instance, in Ref. [19]. These provide the total contributions to the relevant form factors F_L and F_R that are related to the decay amplitude F by

$$iF = -ig \bar{u}_{l_k}(-p_2)(F_L P_L + F_R P_R) v_{l_m}(p_3), \tag{23}$$

where

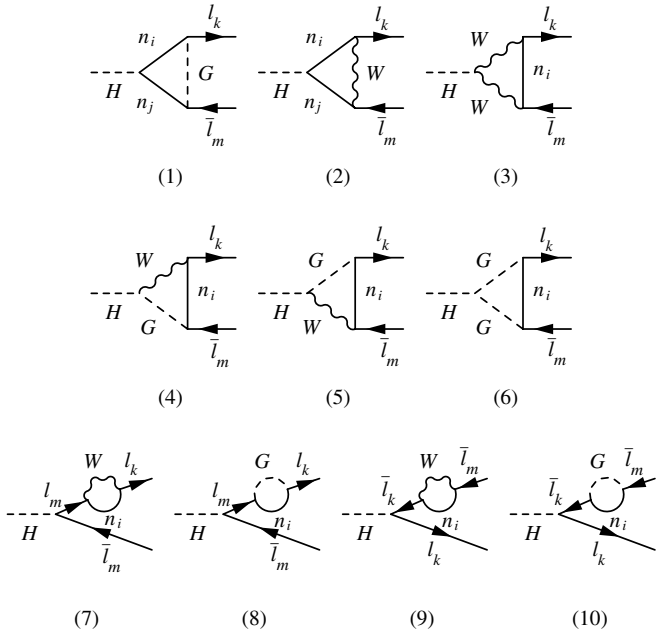

FIG. 1. One-loop diagrams for the LFVHD in the SM-seesaw model.

$$F_L = \sum_{i=1}^{10} F_L^{(i)}, \qquad F_R = \sum_{i=1}^{10} F_R^{(i)}, \tag{24}$$

and $p_1 = p_3 - p_2$ is the ingoing Higgs boson momentum.

The LFVHD widths can be obtained finally from these form factors by

$$\begin{aligned}\Gamma(H \to l_k \bar{l}_m) = & \frac{g^2}{16\pi m_H} \\ & \times \sqrt{\left[1 - \left(\frac{m_{l_k} + m_{l_m}}{m_H}\right)^2\right]\left[1 - \left(\frac{m_{l_k} - m_{l_m}}{m_H}\right)^2\right]} \\ & \times [(m_H^2 - m_{l_k}^2 - m_{l_m}^2)(|F_L|^2 + |F_R|^2) \\ & - 4 m_{l_k} m_{l_m} \mathrm{Re}(F_L F_R^*)].\end{aligned} \tag{25}$$

Notice that, since we will consider complex R matrices, the corresponding decay widths for the CP conjugate states, in general, can be different. We do not study here these CP conjugate decays and concentrate on the $H \to \tau\bar{\mu}$, $\tau\bar{e}$, $\mu\bar{e}$ decays.

Regarding the analytical results, it is worth mentioning that we have checked the finiteness of the total form factors F_L and F_R. When summing up all involved indices in each diagram, we find out, in agreement with Ref. [12], that the only divergent diagrams left are 1, 8, and 10 and these divergences cancel among each other, providing the expected finite result.

We next present the numerical results. The one-loop functions $C_0, B_0, \ldots$ have been evaluated with the MATHEMATICA package of Ref. [20]. For the numerical estimates of the branching ratios we evaluate the coupling matrices of Eq. (22) in terms of ξ, for the particular input values of m_D and m_M that are compatible with the neutrino data. That is, we get m_D from Eq. (10), for the two scenarios A and B and for various choices of the input masses $m_{N_{1,2,3}}$ and the matrix R, as explained in Sec. II, and take $m_{M_i} = m_{N_i}$. The total width has been evaluated with the HDECAY program [21].

The main conclusion from the results in Table I is that the LFVHD rates in the SM-seesaw are extremely small and depend strongly on the Majorana mass scale. In all scenarios considered here and for large m_N, say, larger than 10^4 GeV, the decay rates decrease with the Majorana mass, as $\sim(1/m_M^2)$, and therefore they become very small for very large masses of the heavy neutrinos. This behavior is easily explained by the fact that the dominant contributions to the form factors are proportional to $\xi\xi^+ \sim \mathcal{O}(m_D^2/m_M^2)$ and m_D being obtained by Eq. (10) goes as $m_D \sim m_M^{1/2}$, so that the form factors scale as $F \sim 1/m_M$ and, consequently, the branching ratios as $\mathrm{BR} \sim 1/m_M^2$. That is, we get decoupling of the heavy neutrinos. We have checked numerically this behavior, as can be seen in Fig. 2. Incidentally, it should be mentioned that, since we are keeping the masses of the light neutrinos nonvanishing, the asymptotic value is not exactly zero but an extremely small value.

The R matrix that appears in the relation between m_D and m_M can also be relevant in some scenarios. In particular, if the θ_i angles are complex, the R-matrix elements can have large modulus, the derived m_D can increase relevantly, and, therefore, the decay rates can be much larger, although still very small. This can be seen clearly by comparing the first and second columns of Table I. Notice also that, due to the leptonic mass hierarchy, the

TABLE I. Branching ratios of the LFVHD in the SM-seesaw, for scenarios A and B and for various choices of the heavy neutrino masses. The R matrix is chosen as in case 0 and case 1 with $\theta_1 = \theta_2 = \theta_3 = \pi/3e^{i\pi/3}$. Here $\mathrm{BR}_{12} = \mathrm{BR}(H \to \mu\bar{e})$, $\mathrm{BR}_{13} = \mathrm{BR}(H \to \tau\bar{e})$, $\mathrm{BR}_{23} = \mathrm{BR}(H \to \tau\bar{\mu})$, and $m_H = 115$ GeV.

		R_0	R_1
(A)	BR_{12}	3×10^{-42}	2×10^{-32}
$m_{N_{1,2,3}} = 10^3$ GeV	BR_{13}	1×10^{-39}	2×10^{-30}
	BR_{23}	3×10^{-36}	3×10^{-30}
(A)	BR_{12}	1×10^{-46}	1×10^{-36}
$m_{N_{1,2,3}} = 10^6$ GeV	BR_{13}	3×10^{-44}	1×10^{-34}
	BR_{23}	1×10^{-40}	1×10^{-34}
(B)	BR_{12}	1×10^{-38}	1×10^{-35}
$m_{N_{1(2)}} = 1(5) \times 10^3$ GeV	BR_{13}	1×10^{-36}	3×10^{-33}
$m_{N_3} = 1 \times 10^5$ GeV	BR_{23}	1×10^{-37}	3×10^{-32}
(B)	BR_{12}	4×10^{-39}	1×10^{-36}
$m_{N_{1(2)}} = 1(5) \times 10^4$ GeV	BR_{13}	1×10^{-37}	1×10^{-34}
$m_{N_3} = 1 \times 10^6$ GeV	BR_{23}	1×10^{-37}	2×10^{-33}

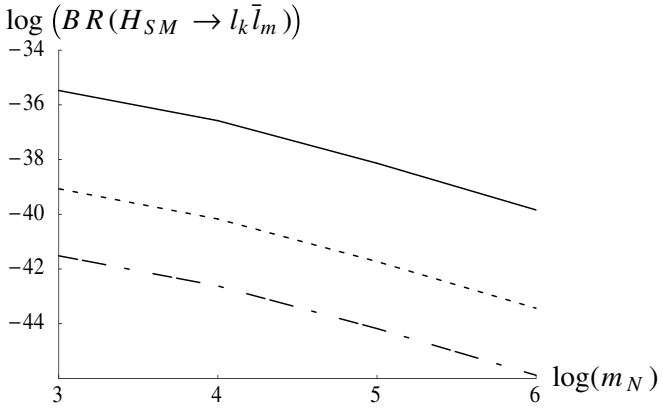

FIG. 2. Dependence of the LFVHD ratios in the SM-seesaw with m_N (GeV) in scenario A with degenerate heavy neutrinos. Solid, short-dashed, and long-dashed lines are for BR_{23}, BR_{13}, and BR_{12}, respectively.

larger rates are always obtained for the decays involving the τ lepton.

Therefore, one can conclude that the LFVHD rates in the SM-seesaw are negligibly small and the largest values are for the lowest Majorana mass choices and largest complex angles in the R matrix. These conclusions are valid for both scenarios A and B.

In order to compare these results with the ones obtained in Ref. [12], it has to be taken into account that in their computation the seesaw parameter ξ was fixed to a particular numerical value, so that, for large m_M, m_D scales as $m_D \sim m_M$, in contrast to our case where, as we have said, $m_D \sim m_M^{1/2}$. These different assumptions on the relation between m_D and m_M give rise to very different decay rates. The branching ratios in their computation grow instead with m_M; thus, by providing very large values to the Dirac masses (i.e., the Yukawa couplings get strong as $m_N \simeq m_M$ increases), they obtained much larger values for the branching ratios. For a fixed neutrino mass m_N, the only way to reach these large values for the Dirac masses in our scenario is by considering extremely large complex R-matrix elements. As an example, in scenario A and case 1 with $m_{N_i} = 1$ TeV and $\theta_{1,2,3} \sim 5i$, we obtain $|m_D| \sim 200$ GeV and $BR_{23} \sim 10^{-6}$, which are closer to the predicted values in Ref. [12]. But this is not a natural assumption in seesaw models since it requires a strong fine-tuning in the choice of the m_D and m_M matrices.

We also include next, for comparison, the numerical results for the LFVHD branching ratios in the case of Dirac neutrinos and for $m_H = 115$ GeV. For the two scenarios A and B they are, correspondingly,

$$\mathrm{BR}(H \to \mu\bar{e}) = 2 \times 10^{-62}(\mathrm{A}),\, 2 \times 10^{-62}(\mathrm{B}),$$

$$\mathrm{BR}(H \to \tau\bar{e}) = 1 \times 10^{-60}(\mathrm{A}),\, 1 \times 10^{-60}(\mathrm{B}),$$

$$\mathrm{BR}(H \to \tau\bar{\mu}) = 3 \times 10^{-56}(\mathrm{A}),\, 2 \times 10^{-56}(\mathrm{B}).$$

As we can see, these ratios are negligible and much smaller than in the case of Majorana neutrinos. We also learn from our results than the ratios undergo a strong cancellation when the internal neutrinos in the loop diagrams are summed over the three generations. This suppression is similar to the Glashow, Iliopoulos, and Maiani suppression mechanism of the quark sector. Notice that our rates disagree in many orders of magnitude with the results of Ref. [14], where a prediction of $\mathrm{BR}(H \to \tau\bar{\mu}) \sim 6 \times 10^{-7}$ was presented. We believe that this disagreement could be due to the above mentioned strong cancellations which are not taking place in their case.

IV. LEPTON FLAVOR VIOLATING HIGGS DECAYS IN THE MSSM-SEESAW

In this section we study the lepton flavor violating Higgs decays within the context of the MSSM-seesaw model. We first analyze the various sources of lepton flavor changing processes in this model, and next we compute the LFVHD partial widths and branching ratios for the three neutral MSSM Higgs boson decays, $\Gamma(H_x \to l_k\bar{l}_m)$ with $H_x = h_0, H_0, A_0$, and $l_k\bar{l}_m = \tau\bar{\mu}, \tau\bar{e}, \mu\bar{e}$. We also analyze in parallel the lepton flavor changing $l_j \to l_i\gamma$ decays and explore the maximum predicted rates for LFVHD, mainly for $H^0, A^0 \to \tau\bar{\mu}$ decays, by requiring the $\mathrm{BR}(l_j \to l_i\gamma)$ rates to be within the experimentally allowed range. We use the present experimental upper bounds given, respectively, by $|\mathrm{BR}(\mu \to e\gamma)| < 1.2 \times 10^{-11}$ [9], $|\mathrm{BR}(\tau \to \mu\gamma)| < 3.1 \times 10^{-7}$ [10], and $|\mathrm{BR}(\tau \to e\gamma)| < 2.7 \times 10^{-6}$ [11].

A. Sources of LFV interactions in the MSSM-seesaw

In the MSSM-seesaw model there are two sources of lepton flavor changing processes. The first one is induced from the nonvanishing mixing in the light neutrino sector, that is, from the off-diagonal elements of the U_{MNS} matrix. We have already seen in the previous section that these elements induce, via charged currents, intergenerational interactions of the type $W^\pm - l_i - \nu_j$ (and the corresponding $G^\pm - l_i - \nu_j$) with $i \neq j$. These will be generated in the MSSM-seesaw as well, but in addition, there will appear new tree-level LFV interactions involving neutrinos, as, for instance, those with charginos $\tilde{\chi}^\pm$ and charged sleptons $\tilde{l}$, $\tilde{\chi}^\pm - \tilde{l}_i - \nu_j$ with $i \neq j$, and those with neutralinos $\tilde{\chi}^0$ and sneutrinos $\tilde{\nu}$, $\tilde{\chi}^0 - \tilde{\nu}_i - \nu_j$ with $i \neq j$. From the operational point of view, these effects are introduced by the explicit factors of the U_{MNS} matrix elements in the corresponding couplings when referred to the physical basis. Because of the extended Higgs sector of the MSSM-seesaw, there will be additional intergenerational couplings of the type $H^\pm l_i \nu_j$ with similar $(U_{\mathrm{MNS}})_{ij}$ factors.

All of the previous intergenerational couplings can induce important contributions to LFV processes with external SM leptons. In the following we will refer to the radiatively induced flavor changing effects from the

$(U_{\rm MNS})_{ij}$ factors in the couplings as $U_{\rm MNS}$ effects. For the case under study here of LFVHD, the couplings inducing these $U_{\rm MNS}$ effects are just $W^{\pm} l_i \nu_j$, $G^{\pm} l_i \nu_j$, and $H^{\pm} l_i \nu_j$. The size of the generated effects from the $W^{\pm} l_i \nu_j$ and $G^{\pm} l_i \nu_j$ couplings are expected to be as small as in the SM-seesaw case. The only difference comes from the different couplings of the internal particles to the external h_0, H_0, and A_0 Higgs bosons as compared to those of the SM Higgs boson H, but this difference will not change relevantly the small size of the generated ratios. On the other hand, the generated effects from the $H^{\pm} l_i \nu_j$ couplings are new with respect to the SM-seesaw case. We have numerically estimated the size of the contributions to the LFVHD branching ratios from all the one-loop diagrams with internal $H^{\pm}$, $W^{\pm}$, and $G^{\pm}$, and we have found that they are indeed always negligibly small. We will in consequence ignore all these contributions in the following.

The second source of LFV processes in the MSSM-seesaw is genuine in SUSY models and comes from the misalignment between the rotations leading to the mass eigenstate basis of sleptons relative to that of leptons. This misalignment is radiatively generated in the SUSY-seesaw models from the Yukawa couplings of the Majorana neutrinos and can be sizable in both the charged slepton and sneutrino sectors. Once one rotates the so-generated flavor nondiagonal charged slepton and sneutrino mass matrices to the physical diagonal ones, some intergenerational couplings involving SUSY particles are generated. For the case of LFVHD, the involved couplings are $\tilde{\chi}^{\pm} l_i \tilde{\nu}_j$ and $\tilde{\chi}^0 l_i \tilde{l}_j$ with $i \neq j$. These generated effects from lepton-slepton misalignment will be called in the following misalignment effects. All these couplings will induce via loops of SUSY particles relevant contributions to the LFVHD rates as will be shown later on.

The LFV effects from misalignment are usually implemented in the seesaw models in the language of the RGE and can be summarized as follows. One starts with universal soft-SUSY-breaking parameters at the large energies $M_X \gg m_M$ given by

$$\begin{aligned} (m_{\tilde{L}}^2)_{ij} &= M_0^2 \delta_{ij}, \qquad (m_{\tilde{E}}^2)_{ij} = M_0^2 \delta_{ij}, \\ (m_{\tilde{M}}^2)_{ij} &= M_0^2 \delta_{ij}, \qquad (A_l)_{ij} = A_0 (Y_l)_{ij}, \\ (A_\nu)_{ij} &= A_0 (Y_\nu)_{ij}, \end{aligned} \tag{26}$$

where M_0 and A_0 are the universal soft-slepton mass and soft-trilinear coupling, respectively. Y_l is the Yukawa coupling matrix of the charged leptons, which is flavor diagonal in the basis chosen here, $(Y_l)_{ij} = Y_{l_i} \delta_{ij}$ with $Y_{l_i} = m_{l_i}/v_1$, and $v_1 = v \cos\beta$. Y_ν is the Yukawa coupling matrix of the neutrinos and is given by $(Y_\nu)_{ij} = (m_D)_{ij}/v_2$, with $v_2 = v \sin\beta$.

The effect of the RGE running from M_X down to m_M on the off-diagonal soft parameters of the charged slepton sector, to one loop and in the leading-log approximation, is then described by

$$\begin{aligned} (\Delta m_{\tilde{L}}^2)_{ij} &= -\frac{1}{8\pi^2} (3M_0^2 + A_0^2)(Y_\nu^* L Y_\nu^T)_{ij}, \\ (\Delta A_l)_{ij} &= -\frac{3}{16\pi^2} A_0 Y_{l_i} (Y_\nu^* L Y_\nu^T)_{ij}, \\ (\Delta m_{\tilde{E}}^2)_{ij} &= 0; \\ L_{kl} &\equiv \log\left(\frac{M_X}{m_{M_k}}\right) \delta_{kl}. \end{aligned} \tag{27}$$

Notice that our notation is slightly different from the usual one in that $Y_\nu \leftrightarrow Y_\nu^T$. For all the numerical estimates in this work, we use $M_X = 2 \times 10^{16}$ GeV and, for simplicity, we will assume $A_0 = 0$. Thus, we consider flavor changing only in the LL sector, which is known to be a very good approximation within the context of the seesaw model. In fact, we have checked that even for values as large as $A_0 = M_0 = 1$ TeV the size of the corresponding flavor changing dimensionless parameters in the LR sector are always smaller than the LL ones in more than 3 orders of magnitude. Notice also that, in addition to the previously mentioned $U_{\rm MNS}$ factors, which, as we have said, are not relevant for the present computation of the LFVHD rates, there is an extra dependence on $U_{\rm MNS}$ via the Y_ν couplings or, equivalently, via the m_D matrix as given in Eq. (10). Thus, even if we fixed $U_{\rm MNS}$ to the unit matrix, there could still be flavor changing effects from misalignment via the R matrix. Conversely, if we fixed R to the unit matrix, there could still be flavor changing effects from misalignment via the $U_{\rm MNS}$ matrix in m_D. Finally, notice that the effect of neutrino Yukawa couplings, via RGE running from M_X down to m_M, on the diagonal entries of the squared-mass matrices are small and have been neglected in this work. On the other hand, as we have previously said, we have included the effects of the RGE running from m_W up to m_N on the neutrino masses m_{ν_i} $(i = 1, 2, 3)$ and the $U_{\rm MNS}$ matrix elements, and we have used the corresponding corrected parameters in Eq. (10) to evaluate the Yukawa couplings Y_ν.

In order to estimate the size of the misalignment effects, we first study in detail the dependence of the flavor changing dimensionless parameters, in the LL sector, defined as $\lambda_{ij} \equiv (\Delta m_{\tilde{L}}^2)_{ij}/M_0^2$, as a function of the seesaw parameters. We show in Figs. 3 and 4 the predictions of the λ_{ij} parameter as a function of the seesaw parameters and in some selected examples within the scenarios described above. We show in Fig. 3(a) the dependence of $|\lambda_{ij}|$ with m_N, for scenario A and real R. Notice that in this case, the λ_{ij} turn out to be independent on R, so this figure applies both to case 0 and to case 1 with θ_i real. As can be seen, the three $|\lambda_{ij}|$ grow with m_N and the largest one, which is $|\lambda_{23}|$, reaches values up to 2.4×10^{-3} for $m_N = 10^{14}$ GeV. The size of $|\lambda_{12}|$ can reach values up to 3.8×10^{-5} for $m_N = 10^{14}$ GeV and correspondingly for $|\lambda_{13}| \simeq |\lambda_{12}|$. The size

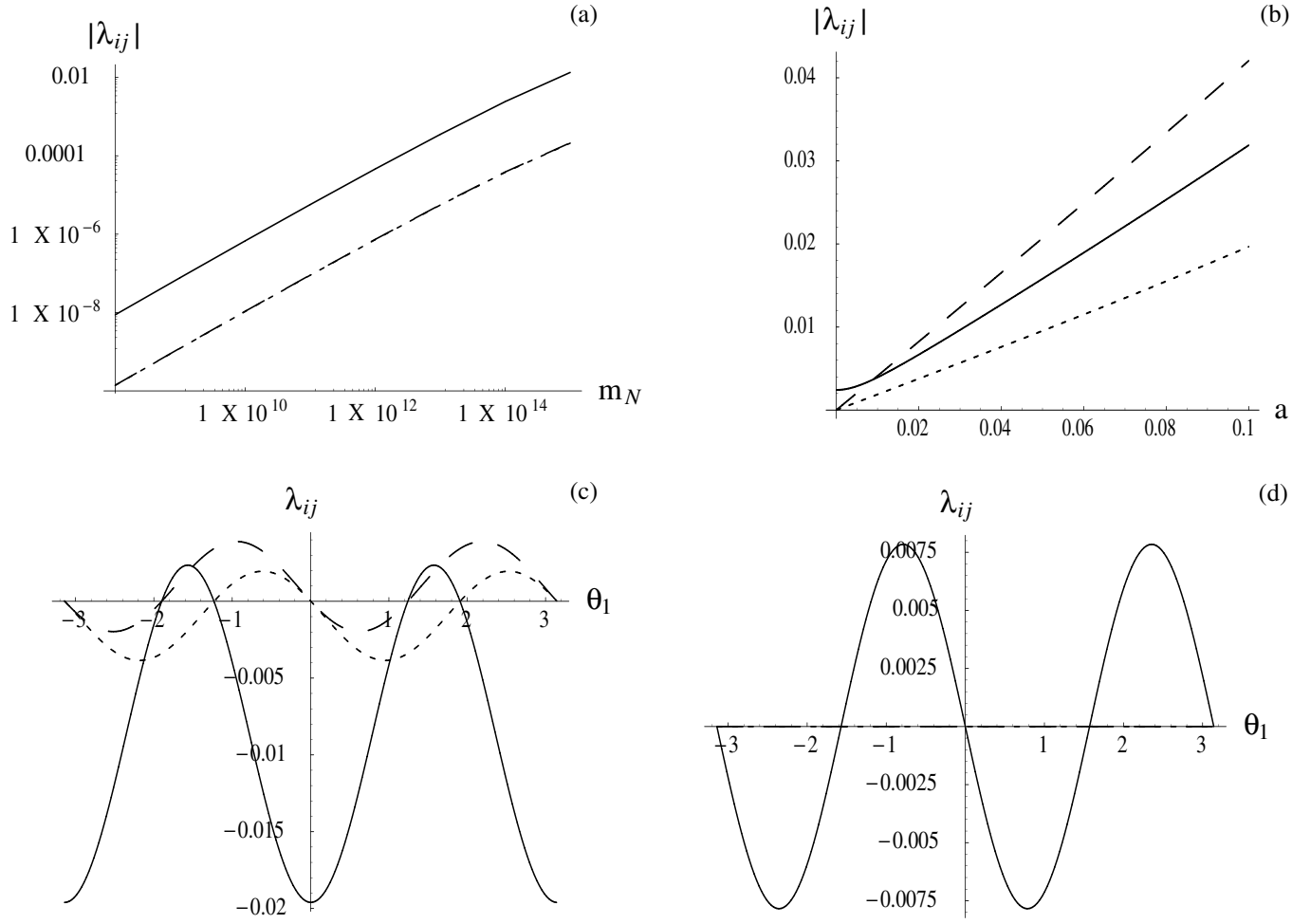

FIG. 3. Dependence of λ_{ij} with the seesaw parameters. Solid, long-dashed, and short-dashed lines are for λ_{23}, λ_{13}, and λ_{12}, respectively. (a) Dependence with m_N in scenario A for real R. (b) Dependence with the a parameter in scenario A with $m_N = 10^{14}$ GeV and complex R, for case 2 with $a = b = c$. (c) Dependence with real θ_1 in scenario B, case 1, for $(m_{N_1}, m_{N_2}, m_{N_3}) = (10^8, 2 \times 10^8, 10^{14})$ GeV and $\theta_2 = \theta_3 = 0$. (d) Same as in (c) but for $U_{\rm MNS} = 1$. In all plots here, $\tan\beta = 35$.

of the λ_{ij} in this scenario with degenerate heavy neutrinos can obviously be increased if R is assumed instead to be complex. In this case, the λ_{ij} are, in general, complex numbers. As an example, we show in Fig. 3(b) the dependence of $|\lambda_{ij}|$, in scenario A with $m_N = 10^{14}$ GeV, on the parameter a of case 2, for $a = b = c$. The size of $|\lambda_{ij}|$ increases clearly with a and, for the studied range, $|\lambda_{12}|$ can be as large as 2×10^{-2}. In particular, for values of $|abc| \simeq 10^{-5}$ that generate successful baryogenesis [8], the generated $|\lambda_{ij}|$ are still large, namely, $|\lambda_{12}| = 4 \times 10^{-3}$. Notice also that the relative size of the different λ_{ij} changes with respect to Fig. 3(a). The main problem with this scenario A and R complex, with the parametrization of case 2, is that for most choices of the relevant parameters, m_N, a, b, and c, producing successful baryogenesis, the size of the generated λ_{12} is too large and leads to large $\mu \to e\gamma$ decay rates [8] clearly above the present experimental bound of $\mathrm{BR}(\mu \to e\gamma) < 1.2 \times 10^{-11}$ [9]. We have also studied scenario A with complex R given by the parametrization of case 1 and have found that for most choices of the θ_i complex angles the three λ_{12}, λ_{13}, and λ_{23} have comparable sizes and therefore, the required large λ_{23} values leading to large $H \to \tau\bar{\mu}$ ratios imply again experimentally unallowed $\mu \to e\gamma$ ratios. Therefore, we will not consider scenario A with complex R anymore in the following.

The case of hierarchical neutrinos is shown in Figs. 3(c) and 3(d) for real R and in Fig. 4 for complex R with the parametrization of case 1. In Fig. 3(c) it is plotted the dependence with real θ_1 for scenario B with $(m_{N_1}, m_{N_2}, m_{N_3}) = (10^8, 2 \times 10^8, 10^{14})$ GeV and $\theta_2 = \theta_3 = 0$. We see that λ_{23} is the largest one and reaches negative values up to -1.96×10^{-2} at the points $\theta_1 = 0, \pm\pi$, precisely where λ_{12} and λ_{13} vanish. These points are therefore particularly interesting for the LFVHD rates since they will lead to the largest ratios for $H \to \tau\bar{\mu}$ while keeping $\mu \to e\gamma$, $\tau \to e\gamma$ extremely small and, as we will see later, $\tau \to \mu\gamma$ still compatible with data. Notice that

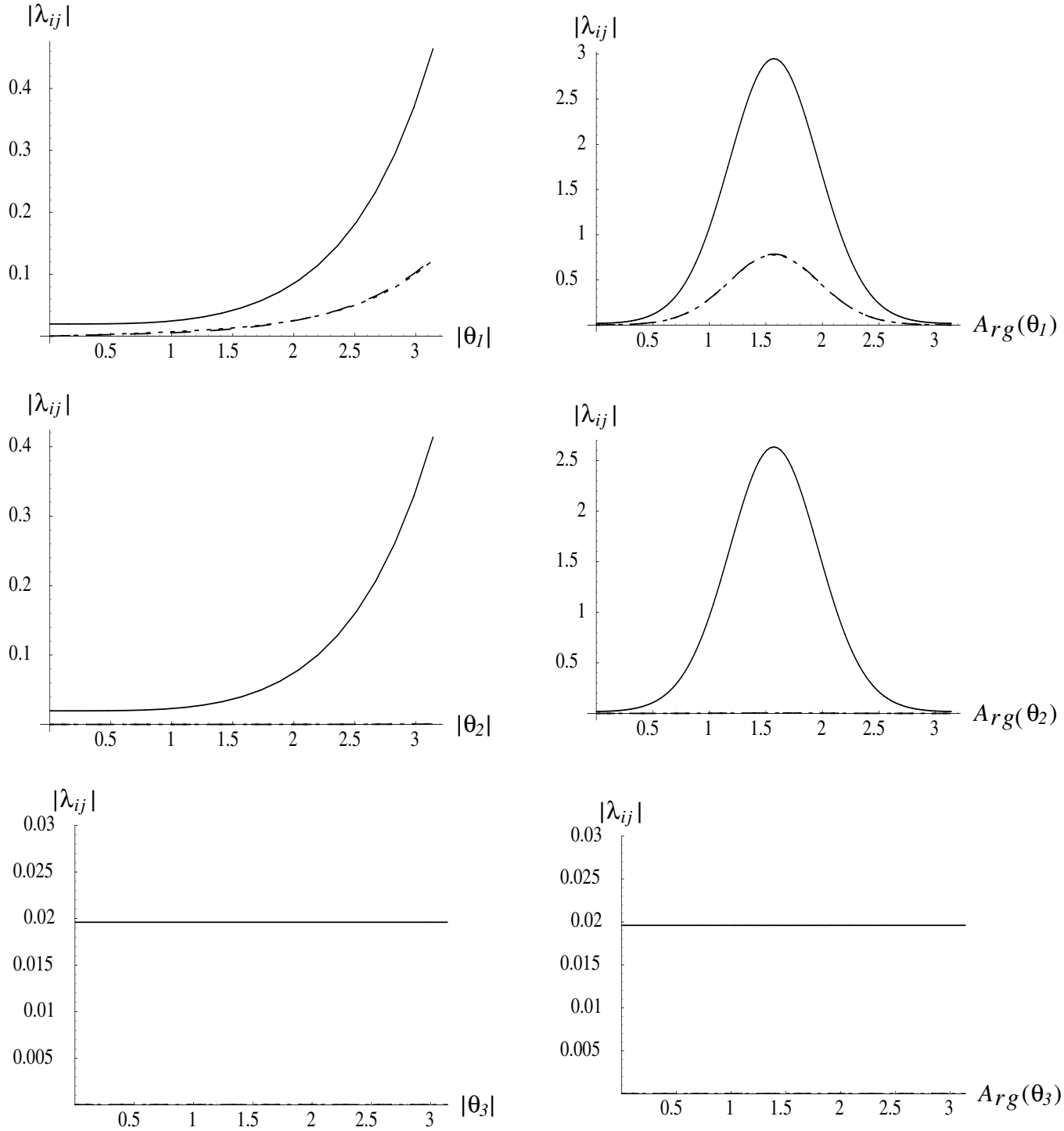

FIG. 4. Dependence of $|\lambda_{ij}|$ with the seesaw parameters for complex θ_i. Solid, long-dashed, and short-dashed lines (the two latter being undistinguishable in the plots) are for $|\lambda_{23}|$, $|\lambda_{13}|$, and $|\lambda_{12}|$, respectively. Left panels: Dependence with $|\theta_1|$, $|\theta_2|$, and $|\theta_3|$, respectively in scenario B, case 1. We take $\mathrm{Arg}(\theta_i) = \pi/4$, correspondingly, and the rest of the angles are set to zero. Right panels: Dependence with $\mathrm{Arg}(\theta_1)$, $\mathrm{Arg}(\theta_2)$, and $\mathrm{Arg}(\theta_3)$, respectively, in scenario B, case 1. We take $|\theta_i| = \pi$, correspondingly, and the rest of the angles are set to zero. In all plots here, $(m_{N_1}, m_{N_2}, m_{N_3}) = (10^8, 2 \times 10^8, 10^{14})$ GeV and $\tan\beta = 35$.

the point $\theta_1 = 0$ in Fig. 3(c) corresponds to the reference case 0 with $R = 1$ and, therefore, represents the situation where the U_{MNS} matrix is the only origin for flavor changing. This means that our experimental input for the U_{MNS} matrix generates by itself sizable rates for lepton flavor violating decays involving the second and third generations. The alternative situation where just the R matrix is generating the lepton flavor violating decays is illustrated

in Fig. 3(d). Here we show the λ_{ij} dependence with θ_1 for $\theta_2 = \theta_3 = 0$ and $U_{\rm MNS} = 1$. We see that $|\lambda_{23}|$ reaches values up to about 7.8×10^{-3}, whereas λ_{12} and λ_{13} vanish for all θ_1. By comparing these two situations we can infer that, for the case of real R with $\theta_1 \neq 0$ and $\theta_2 = \theta_3 = 0$, the induced misalignment effect between the second and third generations from the experimental $U_{\rm MNS}$ is relevant and can be even larger than the effect from R.

We have also studied the alternative choices for real R with $\theta_2 \neq 0$, $\theta_1 = \theta_3 = 0$, and with $\theta_3 \neq 0$, $\theta_1 = \theta_2 = 0$, although the corresponding plots are not shown here for brevity. We find a λ_{23} dependence on θ_2 very similar to that on θ_1, with maximum negative λ_{23} values at $\theta_2 = 0, \pm\pi$ of -1.96×10^{-2}. In contrast, λ_{12} and λ_{13} now take very small values whose maxima are 2.4×10^{-5}. Regarding the dependence with θ_3 a different situation is found, where the three λ_{12}, λ_{13}, and λ_{23} are approximately constant with θ_3 and take the values $\lambda_{23} = -1.96 \times 10^{-2}$ and $\lambda_{13} \simeq \lambda_{12} = 2.4 \times 10^{-5}$, respectively.

The case of hierarchical neutrinos with complex R produces, in most cases, complex λ_{ij} values and their moduli are in general larger than in the case of real R, as can be clearly seen in Fig. 4. Our particular choice for the heavy neutrino masses of $(m_{N_1}, m_{N_2}, m_{N_3}) = (10^8, 2 \times 10^8, 10^{14})$ GeV, where the two lightest neutrinos have similar masses and well below the mass of the heaviest one, produces the specific pattern shown in these plots, where the dependence of $|\lambda_{23}|$ on θ_1, for $\theta_2 = \theta_3 = 0$, and on θ_2, for $\theta_1 = \theta_3 = 0$, are very similar, and $|\lambda_{23}|$ can reach very large values for a large region of the $[|\theta_i|, \mathrm{Arg}(\theta_i)]$, $i = 1, 2$ parameter space. For instance, for fixed $\mathrm{Arg}(\theta_1) = \pi/4$ and $|\theta_1|$ up to π we find $|\lambda_{23}|$ values up to 0.46 and similarly for θ_2. Larger values of $\mathrm{Arg}(\theta_i)$, $i = 1, 2$, produce even larger $|\lambda_{23}|$ and it reaches its maximum at $\mathrm{Arg}(\theta_i) = \pi/2$. In contrast, λ_{12} and λ_{13} reach much smaller values with complex θ_2 than with complex θ_1, being $|\lambda_{12}| \simeq |\lambda_{13}| < 5 \times 10^{-4}$ for $|\theta_2| < \pi$. On the other hand, they depend strongly with complex θ_1 and $|\lambda_{12}|$ can reach too large values, up to $\mathcal{O}(10^{-1})$, in clear conflict with the allowed values by $\mu \to e\gamma$ data. Finally, the behavior with complex θ_3 is very similar to the real case, with the three $|\lambda_{12}|$, $|\lambda_{13}|$, and $|\lambda_{23}|$ being nearly constant with θ_3. Their values are $|\lambda_{23}| = 1.96 \times 10^{-2}$ and $|\lambda_{12}| \simeq |\lambda_{13}| = 2.4 \times 10^{-5}$, respectively.

Regarding the values of the hierarchical heavy neutrino masses, we have also tried other choices in the range 10^8 GeV $\leq m_{N_i} \leq 10^{14}$ GeV and found that, under the favored assumption by baryogenesis of close m_{N_1} and m_{N_2} and much lighter than m_{N_3}, it is the value of this later which matters for $\mathrm{BR}(H \to \tau\bar{\mu})$, leading to larger λ_{23} values for larger m_{N_3} and, therefore, our choice of $(m_{N_1}, m_{N_2}, m_{N_3}) = (10^8, 2 \times 10^8, 10^{14})$ GeV seems to be appropriate. We have checked that alternative choices where m_{N_2} and m_{N_3} are close and much heavier than m_{N_1} lead to a similar situation for $\theta_1 \neq 0$, $\theta_2 = \theta_3 = 0$ than the previous case, but it gives larger predictions for λ_{12} in conflict with $\mu \to e\gamma$ data. For the following predictions of decay rates in the case of hierarchical neutrinos, we will fix the values to $(m_{N_1}, m_{N_2}, m_{N_3}) = (10^8, 2 \times 10^8, 10^{14})$ GeV.

In summary, the case of hierarchical heavy neutrinos leads to larger λ_{ij} values than the degenerate case and, in consequence, larger LFVHD rates. Futhermore, in order to get the largest possible $\mathrm{BR}(H \to \tau\bar{\mu})$ rates while keeping all $\mathrm{BR}(l_j \to l_i\gamma)$ rates within the experimentally allowed regions, the most favorable case of all the studied ones, and for our choice of neutrino masses, is the one with complex $\theta_2 \neq 0$ and $\theta_1 = \theta_3 = 0$.

The next step is the diagonalization of the charged slepton and sneutrino mass matrices leading to the mass eigenvalues and mass eigenstates at the electroweak energy scale. We start with the nondiagonal charged slepton and sneutrino squared-mass matrices that are obtained after the running from M_X to M_W and once the charged leptons and neutrinos have been rotated to the physical basis. For the charged sector, this matrix is referred to as the $(\tilde{e}_L, \tilde{e}_R, \tilde{\mu}_L, \tilde{\mu}_R, \tilde{\tau}_L, \tilde{\tau}_R)$ basis and can be written as follows:

$$M_{\tilde{l}}^2 = \begin{pmatrix} M_{LL}^{ee2} & M_{LR}^{ee2} & M_{LL}^{e\mu 2} & 0 & M_{LL}^{e\tau 2} & 0 \\ M_{RL}^{ee2} & M_{RR}^{ee2} & 0 & 0 & 0 & 0 \\ M_{LL}^{\mu e 2} & 0 & M_{LL}^{\mu\mu 2} & M_{LR}^{\mu\mu 2} & M_{LL}^{\mu\tau 2} & 0 \\ 0 & 0 & M_{RL}^{\mu\mu 2} & M_{RR}^{\mu\mu 2} & 0 & 0 \\ M_{LL}^{\tau e 2} & 0 & M_{LL}^{\tau\mu 2} & 0 & M_{LL}^{\tau\tau 2} & M_{LR}^{\tau\tau 2} \\ 0 & 0 & 0 & 0 & M_{RL}^{\tau\tau 2} & M_{RR}^{\tau\tau 2} \end{pmatrix}, \tag{28}$$

where

$$\begin{aligned} &M_{LL}^{ll2} = m_{\tilde{L},l}^2 + m_l^2 + m_Z^2 \cos 2\beta(-\tfrac{1}{2} + \sin^2\theta_W), \qquad M_{RR}^{ll2} = m_{\tilde{E},l}^2 + m_l^2 - m_Z^2 \cos 2\beta \sin^2\theta_W, \\ &M_{LR}^{ll2} = M_{RL}^{ll2} = m_l(A_l - \mu \tan\beta), \qquad M_{LL}^{e\mu 2} = (\Delta m_{\tilde{L}}^2)_{12}; \qquad M_{LL}^{\mu e 2} = (\Delta m_{\tilde{L}}^2)_{21}, \qquad M_{LL}^{e\tau 2} = (\Delta m_{\tilde{L}}^2)_{13}; \\ &M_{LL}^{\tau e 2} = (\Delta m_{\tilde{L}}^2)_{31}, \qquad M_{LL}^{\mu\tau 2} = (\Delta m_{\tilde{L}}^2)_{23}; \qquad M_{LL}^{\tau\mu 2} = (\Delta m_{\tilde{L}}^2)_{32}. \end{aligned} \tag{29}$$

The soft-SUSY-breaking masses and trilinear couplings above, $m_{\tilde{L},e}$, $m_{\tilde{L},\mu}$, $m_{\tilde{L},\tau}$, and A_l, refer to their corresponding values at the electroweak scale. We got them by solving numerically the RGE with the program MSUSPECT [22] and by imposing the universality conditions at $M_X = 2 \times 10^{16}$ GeV for the sfermion sector, Eq. (26), together with the corresponding ones for the gaugino and Higgs boson sectors, $M_1(M_X) = M_2(M_X) = M_{1/2}$ and

$M_{H_1}(M_X) = M_{H_2}(M_X) = M_0$, respectively. For the gaugino sector, this implies the well known relation at low energies, $M_1(M_W) = \frac{5}{3}(\tan\theta_W)^2 M_2(M_W)$. The value of the supersymmetric μ parameter is extracted as usual from the electroweak breaking condition. We choose in all this paper $\mu > 0$ and do not expect relevant differences for $\mu < 0$.

After diagonalization of the $M_{\tilde{l}}^2$ matrix one gets the physical slepton masses and the six mass eigenstates $(\tilde{l}_1, \ldots, \tilde{l}_6) \equiv \tilde{l}$ which are related to the previous weak eigenstates $(\tilde{e}_L, \ldots, \tilde{\tau}_R) \equiv \tilde{l}'$ by the corresponding 6×6 rotation matrix $\tilde{l}' = R^{(l)}\tilde{l}$.

Regarding the sneutrino sector one proceeds similarly to the charged slepton sector, but now the diagonalization process is simpler because of the involved seesaw matrix ξ which gives rise naturally to a suppression of the RH sneutrino components in the relevant mass eigenstates. This can be easily illustrated in the one generation case, but for three generations one arises to similar conclusions. The sneutrino mass terms of the MSSM-seesaw model can be written in the one generation case [23] as

$$-\mathcal{L}^{\nu}_{\text{mass}} = [\,\text{Re}(\tilde{\nu}_L)\text{Re}(\tilde{\nu}_R)\text{Im}(\tilde{\nu}_L)\text{Im}(\tilde{\nu}_R)\,] \times \begin{pmatrix} M_+^2 & 0 \\ 0 & M_-^2 \end{pmatrix} \begin{bmatrix} \text{Re}(\tilde{\nu}_L) \\ \text{Re}(\tilde{\nu}_R) \\ \text{Im}(\tilde{\nu}_L) \\ \text{Im}(\tilde{\nu}_R) \end{bmatrix}, \tag{30}$$

with

$$M_{\pm}^2 = \begin{bmatrix} m_{\tilde{L}}^2 + m_D - \frac{1}{2}m_Z^2\cos 2\beta & m_D(A_\nu - \mu\cot\beta \pm m_M) \\ m_D(A_\nu - \mu\cot\beta \pm m_M) & m_{\tilde{M}}^2 + m_D^2 + m_M^2 \pm 2B_M m_M \end{bmatrix}. \tag{31}$$

Notice that now there are several mass scales involved, the soft-SUSY-breaking parameters $m_{\tilde{L}}$, $m_{\tilde{M}}$, B_M, and A_ν, the Dirac mass m_D, the μ-mass parameter, the Z boson mass m_Z, and the Majorana neutrino mass m_M. Our basic assumption in all this paper is that m_M is much heavier than the other mass scales involved (obviously, except M_X), $m_M \gg m_D, m_Z, \mu, m_{\tilde{L}}, m_{\tilde{M}}, A_\nu, B_M$. The size of B_M has been discussed in the literature [23] and seems more controversial. For simplicity, we shall assume here that this is also smaller than m_M. In this situation, the diagonalization of the previous sneutrino squared-mass matrix is simpler and leads to four mass eigenstates, two of which are light, ξ_1^l, ξ_2^l, and two heavy, ξ_1^h, ξ_2^h. In the leading orders of the series expansion in powers of ξ the mass eigenstates and their corresponding mass eigenvalues are given by

$$\begin{aligned} &\xi_1^l = \sqrt{2}[\text{Re}(\tilde{\nu}_L) - \xi\text{Re}(\tilde{\nu}_R)]; \qquad \xi_2^l = \sqrt{2}[\text{Im}(\tilde{\nu}_L) - \xi\text{Im}(\tilde{\nu}_R)], \qquad \xi_1^h = \sqrt{2}[\text{Re}(\tilde{\nu}_R) + \xi\text{Re}(\tilde{\nu}_L)]; \\ &\xi_2^h = \sqrt{2}[\text{Im}(\tilde{\nu}_R) - \xi\text{Im}(\tilde{\nu}_L)], \qquad m^2_{\xi^l_{1,2}} = m_{\tilde{L}}^2 + \tfrac{1}{2}m_Z^2\cos 2\beta \mp 2m_D(A_\nu - \mu\cot\beta - B_N)\xi, \\ &m^2_{\xi^h_{1,2}} = m_M^2 \pm 2B_M m_M + m_{\tilde{M}}^2 + 2m_D^2. \end{aligned} \tag{32}$$

Here we can see that the heavy states $\xi^h_{1,2}$ will couple very weakly to the rest of particles of the MSSM via their $\tilde{\nu}_L$ component, which is highly suppressed by the small factor ξ and, therefore, it is a good approximation to ignore them and keep just the light states $\xi^l_{1,2}$, which are made mainly of $\tilde{\nu}_L$ and its complex conjugate $\tilde{\nu}_L^*$. Now, by working in this simplified basis but applied to the three generations case, which we write for short $\tilde{\nu}'_\alpha$ ($\alpha = 1, 2, 3$), the relevant 3×3 sneutrino squared-mass matrix can be written as follows:

$$M_{\tilde{\nu}}^2 = \begin{bmatrix} m_{\tilde{L},e}^2 + \frac{1}{2}m_Z^2\cos 2\beta & (\Delta m_{\tilde{L}}^2)_{12} & (\Delta m_{\tilde{L}}^2)_{13} \\ (\Delta m_{\tilde{L}}^2)_{21} & m_{\tilde{L},\mu}^2 + \frac{1}{2}m_Z^2\cos 2\beta & (\Delta m_{\tilde{L}}^2)_{23} \\ (\Delta m_{\tilde{L}}^2)_{31} & (\Delta m_{\tilde{L}}^2)_{32} & m_{\tilde{L},\tau}^2 + \frac{1}{2}m_Z^2\cos 2\beta \end{bmatrix}, \tag{33}$$

where $m_{\tilde{L}_l}^2$ and $(\Delta m_{\tilde{L}}^2)_{ij}$ are the same as in the previous charged slepton squared-mass matrix. After diagonalization of the $M_{\tilde{\nu}}^2$ matrix one gets the relevant physical sneutrino masses and eigenstates $\tilde{\nu}_\beta$ ($\beta = 1, 2, 3$) which are related to the previous states $\tilde{\nu}'_\alpha$ by the corresponding 3×3 rotation matrix, $\tilde{\nu}' = R^{(\nu)}\tilde{\nu}$.

To end this subsection, we summarize all the interaction terms that are relevant for the computation of the LFVHD rates. We present these interactions in the physical mass eigenstate basis and will perform all the computations in this basis. It implies diagonalization in all the involved SUSY sectors, charged sleptons, sneutrinos, charginos, neutralinos, and Higgs bosons. The SUSY-electroweak interaction terms among charginos, leptons, and sneutrinos and among neutralinos, leptons, and sleptons that are responsible for the LFVHD are as follows:

$$\mathcal{L}_{\tilde{\chi}_j^- l \tilde{\nu}_\alpha} = -g\bar{l}[A^{(l)}_{L\alpha j}P_L + A^{(l)}_{R\alpha j}P_R]\tilde{\chi}_j^- \tilde{\nu}_\alpha + \text{H.c.},$$
$$\mathcal{L}_{\tilde{\chi}_a^0 l \tilde{l}_\alpha} = -g\bar{l}[B^{(l)}_{L\alpha a}P_L + B^{(l)}_{R\alpha a}P_R]\tilde{\chi}_a^0 \tilde{l}_\alpha + \text{H.c.}, \quad (34)$$

where the coupling factors $A^{(l)}_{L\alpha j}$, $A^{(l)}_{R\alpha j}$, $B^{(l)}_{L\alpha a}$, and $B^{(l)}_{R\alpha a}$ are given in Appendix B.

The other interaction terms that enter in the computation of the LFVHD rates are the Higgs–lepton–lepton, Higgs–sneutrino–sneutrino, Higgs–slepton–slepton, Higgs–chargino–chargino, and Higgs–neutralino–neutralino interactions, reading:

$$\mathcal{L}_{H_x l l} = -gH_x\bar{l}[S^{(x)}_{L,l}P_L + S^{(x)}_{R,l}P_R]l,$$
$$\mathcal{L}_{H_x \tilde{s}_\alpha \tilde{s}_\beta} = -iH_x[g_{H_x \tilde{\nu}_\alpha \tilde{\nu}_\beta}\tilde{\nu}^*_\alpha \tilde{\nu}_\beta + g_{H_x \tilde{l}_\alpha \tilde{l}_\beta}\tilde{l}^*_\alpha \tilde{l}_\beta],$$
$$\mathcal{L}_{H_x \tilde{\chi}_i^- \tilde{\chi}_j^-} = -gH_x\bar{\tilde{\chi}}_i^-[W^{(x)}_{Lij}P_L + W^{(x)}_{Rij}P_R]\tilde{\chi}_j^-, \quad (35)$$
$$\mathcal{L}_{H_x \tilde{\chi}_a^0 \tilde{\chi}_b^0} = -\frac{g}{2}H_x\bar{\tilde{\chi}}_a^0[D^{(x)}_{Lab}P_L + D^{(x)}_{Rab}P_R]\tilde{\chi}_b^0,$$

where the coupling factors $S^{(x)}_{L,q}$, $S^{(x)}_{R,q}$, $g_{H_x \tilde{\nu}_\alpha \tilde{\nu}_\beta}$, $g_{H_x \tilde{l}_\alpha \tilde{l}_\beta}$, $W^{(x)}_{Lij}$, $W^{(x)}_{Rij}$, $D^{(x)}_{Lab}$, and $D^{(x)}_{Rab}$ are collected in Appendix B.

B. LFVHD rates in the MSSM-seesaw

As we have said, the contributions to the LFVHD rates in the MSSM-seesaw come from various sectors. The contributions from the charged Higgs sector and from the SM sector (i.e., $H^\pm$, $W^\pm$, and $G^\pm$) are very small and will not be included here. The main contributions come from the genuine SUSY sector, concretely, from the one-loop diagrams with charginos, neutralinos, sleptons, and sneutrinos shown in Fig. 5.

The contributions of these one-loop diagrams to the form factors are given by

$$F_{L,x} = \sum_{i=1}^{8} F^{(i)}_{L,x}, \qquad F_{R,x} = \sum_{i=1}^{8} F^{(i)}_{R,x}, \quad (36)$$

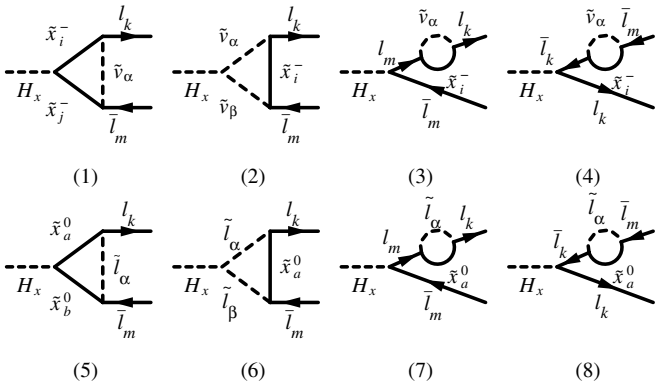

FIG. 5. One-loop diagrams for the LFVHD in the MSSM-seesaw model.

where the analytical results for $F^{(i)}_{L,x}$ and $F^{(i)}_{R,x}$, $i = 1 \ldots 8$ are collected in Appendix B.

The partial widths for the $h^0, H^0, A^0 \to l_k \bar{l}_m$ decays are then finally computed by inserting these form factors correspondingly into Eq. (25). We show in Figs. 6–10 the numerical results of the branching ratios for the LFVHD in the MSSM. The total MSSM Higgs boson widths have been computed with the HDECAY program [21]. We have shown in the plots just the dominant channels, which are $H_x \to \tau\bar{\mu}$, and some comments will be added on the other channels. Similarly, for the comparison with the leptonic radiative decays $l_j \to l_i\gamma$, we will show in the plots the most relevant one, which is $\mu \to e\gamma$ or $\tau \to \mu\gamma$, depending on the case. For the numerical estimates of the $l_j \to l_i\gamma$ branching ratios we use the exact analytical formulas of Ref. [24]. These are expressed in the mass eigenstate basis as well and contain all contributing one-loop diagrams. For the involved $\chi^- l\tilde{\nu}$ and $\chi^0 l\tilde{l}$ couplings we use again the expressions of Appendix B.

The results of the branching ratios for the LFVHD, in the $\tau\bar{\mu}$ channel, as a function of the Majorana mass m_N, in scenario A with degenerate heavy neutrinos and real R, are illustrated in Fig. 6 for several $\tan\beta$ values, $\tan\beta = 3, 10, 30, 50$. The explored range in m_N is from 10^8 GeV up to 10^{14} GeV, which is favorable for baryogenesis. We also show in this figure the corresponding predicted rates for the most relevant lepton decay, which in this case is $\mu \to e\gamma$, and include its upper experimental bound. We have checked that the other channels are well within their experimentally allowed range. From this figure we first see that the branching ratios for the light Higgs boson are smaller than the heavy Higgs ones in about 2 orders of magnitude. The ratios of H_0 and A_0 are very similar in all the plots and, for this scenario, they can reach values up to just 2.2×10^{-10} in the region of high $\tan\beta$ and high m_N. Besides, the rates for $\mu \to e\gamma$ decays are below the upper experimental bound for all explored $\tan\beta$ and m_N values. From these plots we also see clearly the high sensitivity to $\tan\beta$ of the LFVHD rates for all Higgs bosons which, at large $\tan\beta$, scale roughly as $(\tan\beta)^4$, in comparison with the lepton decay rates which scale as $(\tan\beta)^2$. The dependence of both rates on m_N is that induced from the λ_{ij} dependence, and corresponds approximately to what is expected from the mass insertion approximation, where $\text{BR}(H_x \to l_j\bar{l}_i)$, $\text{BR}(l_j \to l_i\gamma) \propto |\lambda_{ij}|^2 \propto |m_N \log(m_N)|^2$.

In regards to the relative importance of the various SUSY sectors to the LFVHD rates, we have found that these are dominated by the chargino contributions, that is, from the loop diagrams (1), (2), (3), and (4) in Fig. 5. For instance, for $m_N = 10^{14}$ GeV, $M_0 = 400$ GeV, and $M_{1/2} = 300$ GeV, we have found the following ratios between the chargino and neutralino contributions to the H^0 form factors: $|F_L^{\tilde{\chi}^-}/F_L^{\tilde{\chi}^0}| = 6.1, 6, 7.3, 23.1$ for $\tan\beta = 3, 10, 30, 50$, respectively, where we have used a simplified

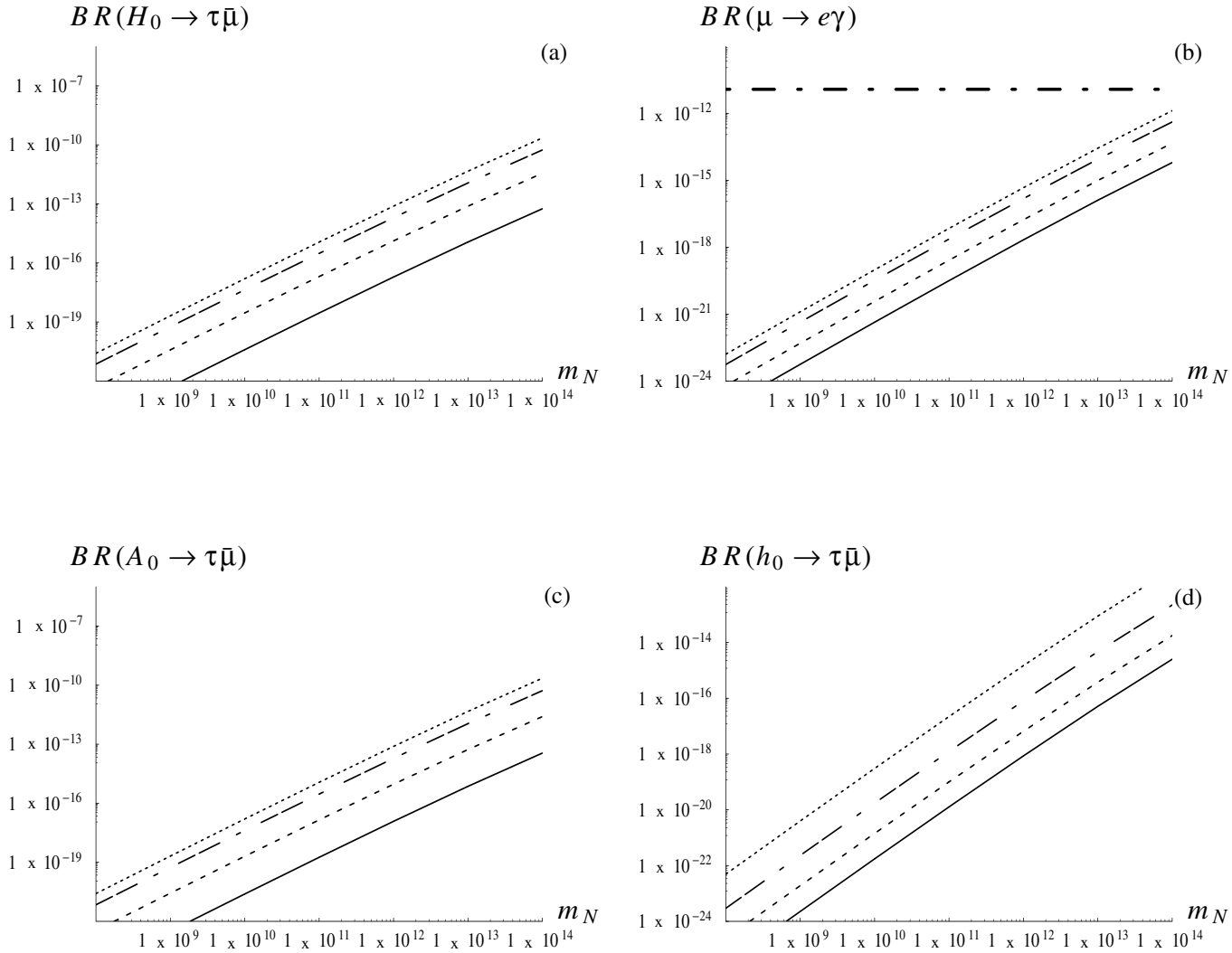

FIG. 6. Dependence of BR($H_x \to \tau\bar{\mu}$) with m_N (GeV) in scenario A with degenerate heavy neutrinos and real R, for several values of $\tan\beta$. (a) $H_x = H_0$, (c) $H_x = A_0$, and (d) $H_x = h_0$. (b) Dependence of BR($\mu \to e\gamma$) with m_N for several values of $\tan\beta$. In all plots, the solid, dashed, dashed-dotted, and dotted lines are the predictions for $\tan\beta = 3$, 10, 30, and 50, respectively. The horizontal line in (b) is the upper experimental bound on BR($\mu \to e\gamma$). The other input parameters are $M_0 = 400$ GeV and $M_{1/2} = 300$ GeV.

notation, $F_L^{\tilde{\chi}^-} = F_{L,H_0}^{(1)} + F_{L,H_0}^{(2)} + F_{L,H_0}^{(3)} + F_{L,H_0}^{(4)}$, $F_L^{\tilde{\chi}^0} = F_{L,H_0}^{(5)} + F_{L,H_0}^{(6)} + F_{L,H_0}^{(7)} + F_{L,H_0}^{(8)}$. Similar $\tilde{\chi}^-/\tilde{\chi}^0$ ratios are found for the corresponding F_R form factors. The relative ratio found of $F_L/F_R \simeq 17$ is nicely explained by the m_τ/m_μ ratio. For the lightest Higgs boson, we find $|F_L^{\tilde{\chi}^-}/F_L^{\tilde{\chi}^0}| = 1.5, 1.4, 1.7, 4$ correspondingly.

Concerning the comparative size of the contributions from the various chargino loop diagrams, we have found that, at large $\tan\beta$, the external leg corrections are clearly the dominant ones. Concretely, for $|(F_{L,H_0}^{(3)} + F_{L,H_0}^{(4)})/F_L^{\tilde{\chi}^-}|$, $|F_{L,H_0}^{(1)}/F_L^{\tilde{\chi}^-}|$, and $|F_{L,H_0}^{(2)}/F_L^{\tilde{\chi}^-}|$, we get the respective percentages 60.6%, 39.3%, and 0.1%, for $\tan\beta = 10$ and 93.8%, 6.2%, 0% for $\tan\beta = 50$.

The branching ratios for the Higgs boson decays into $\tau\bar{e}$ and $\mu\bar{e}$ are much smaller than the $\tau\bar{\mu}$ ones, as expected, and we do not show plots for them. For instance, for $m_N = 10^{14}$ GeV and $\tan\beta = 50$ we find BR($H^{(x)} \to \tau\bar{\mu}$)/BR($H^{(x)} \to \tau\bar{e}$) $= 3.9 \times 10^3$ and BR($H^{(x)} \to \tau\bar{\mu}$)/BR($H^{(x)} \to \mu\bar{e}$) $= 1.3 \times 10^6$ for the three Higgs bosons.

All the previous results are for fixed $M_0 = 400$ GeV and $M_{1/2} = 300$ GeV. The dependence with M_0 and $M_{1/2}$ will be discussed later on within the context of hierarchical neutrinos.

In summary, the LFVHD rates for degenerate heavy neutrinos are very small, at most 2.2×10^{-10}, for the explored range of the seesaw parameters and $\tan\beta$. Obviously, larger values of these LFVHD ratios could be achieved for larger $\tan\beta$ values, but we have not considered them here.

We next present the results for hierarchical neutrinos, scenario B, and use the parametrization of case 1. The results for real and complex R and for the mass hierarchy

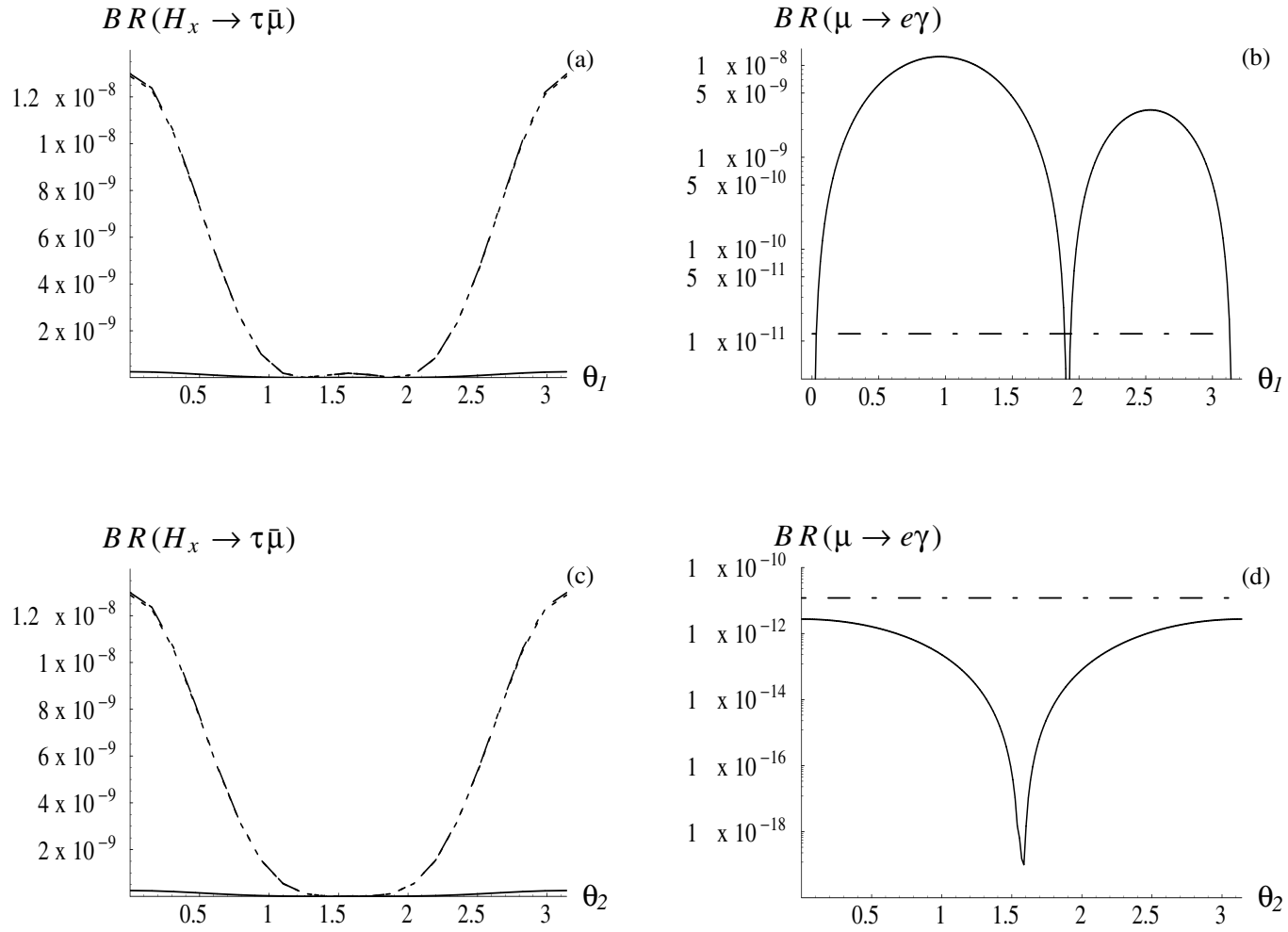

FIG. 7. (a) Dependence of BR($H_x \to \tau\bar{\mu}$) with θ_1. Solid, dashed, and dashed-dotted lines (the two latter undistinguishable here) correspond to $H_x = (h_0, H_0, A_0)$, respectively. (b) Dependence of BR($\mu \to e\gamma$) with θ_1. The horizontal dashed-dotted line is the upper experimental bound. Both panels are in scenario B, case 1 for real $\theta_1 \neq 0$, $(m_{N_1}, m_{N_2}, m_{N_3}) = (10^8, 2 \times 10^8, 10^{14})$ GeV, $\theta_2 = \theta_3 = 0$, $\tan\beta = 50$, $M_0 = 400$ GeV, and $M_{1/2} = 300$ GeV. (c) and (d) are as in (a) and (b), respectively, but for $\theta_2 \neq 0$ and $\theta_1 = \theta_3 = 0$.

$(m_{N_1}, m_{N_2}, m_{N_3}) = (10^8, 2 \times 10^8, 10^{14})$ GeV are shown in Figs. 7 and 8, respectively. From these figures we first confirm that the LFVHD and lepton decay rates are larger in this case than in the degenerate heavy neutrinos one. However, we will get restrictions on the maximum allowed Higgs decay rates coming from the experimental lepton decay bounds. For instance, the case of real θ_1 that is illustrated in Figs. 7(a) and 7(b) for $\tan\beta = 50$, $M_0 = 400$ GeV, and $M_{1/2} = 300$ GeV shows that compatibility with $\mu \to e\gamma$ data occurs only in the very narrow deeps at around $\theta_1 = 0$, 1.9, and π. The presence of these narrow regions where the $\mu \to e\gamma$ rates are drastically suppressed were already pointed out in Ref. [6] and correspond clearly to the minima of $|\lambda_{12}|$ in Fig. 3(c). Notice that it is precisely at the points $\theta_1 = 0, \pi$ where the BR($H_0, A_0 \to \tau\bar{\mu}$) rates reach their maximum values, although these are not large, just about 1.3×10^{-8}. Notice also that these maxima correspond clearly to the maxima of $|\lambda_{23}|$ in Fig. 3(c). We have checked that, for lower $\tan\beta$ values, the allowed regions in θ_1 widen and are placed at the same points, but the corresponding maximum values of the LFVHD rates get considerably reduced. The alternative case of real $\theta_2 \neq 0$ with $\theta_1 = \theta_3 = 0$ is illustrated in Figs. 7(c) and 7(d). We see that the behavior of BR($H_x \to \tau\bar{\mu}$) with θ_2 is very similar to that with θ_1 of Fig. 7(a) and the maximum values of about 1.3×10^{-8} are now placed at $\theta_2 = 0$, π. BR($\mu \to e\gamma$) also reaches its maximum at $\theta_2 = 0, \pi$, but it is still well below the experimental bound. In particular, for $\tan\beta = 50$, $M_0 = 400$ GeV, and $M_{1/2} = 300$ GeV this maximum value is 3×10^{-12}. Notice that the behavior with θ_2 is explained once again in terms of the corresponding λ_{ij} behavior. Regarding the dependence with θ_3, not shown in the plots, a different situation is found, where BR($H_x \to \tau\bar{\mu}$) is approximately constant, and for the heavy Higgs bosons it is around 1.3×10^{-8}. BR($\mu \to e\gamma$), BR($\tau \to \mu\gamma$), and BR($\tau \to e\gamma$) are also approximately constant with θ_3. In addition, we have checked that these three leptonic constant decay rates are

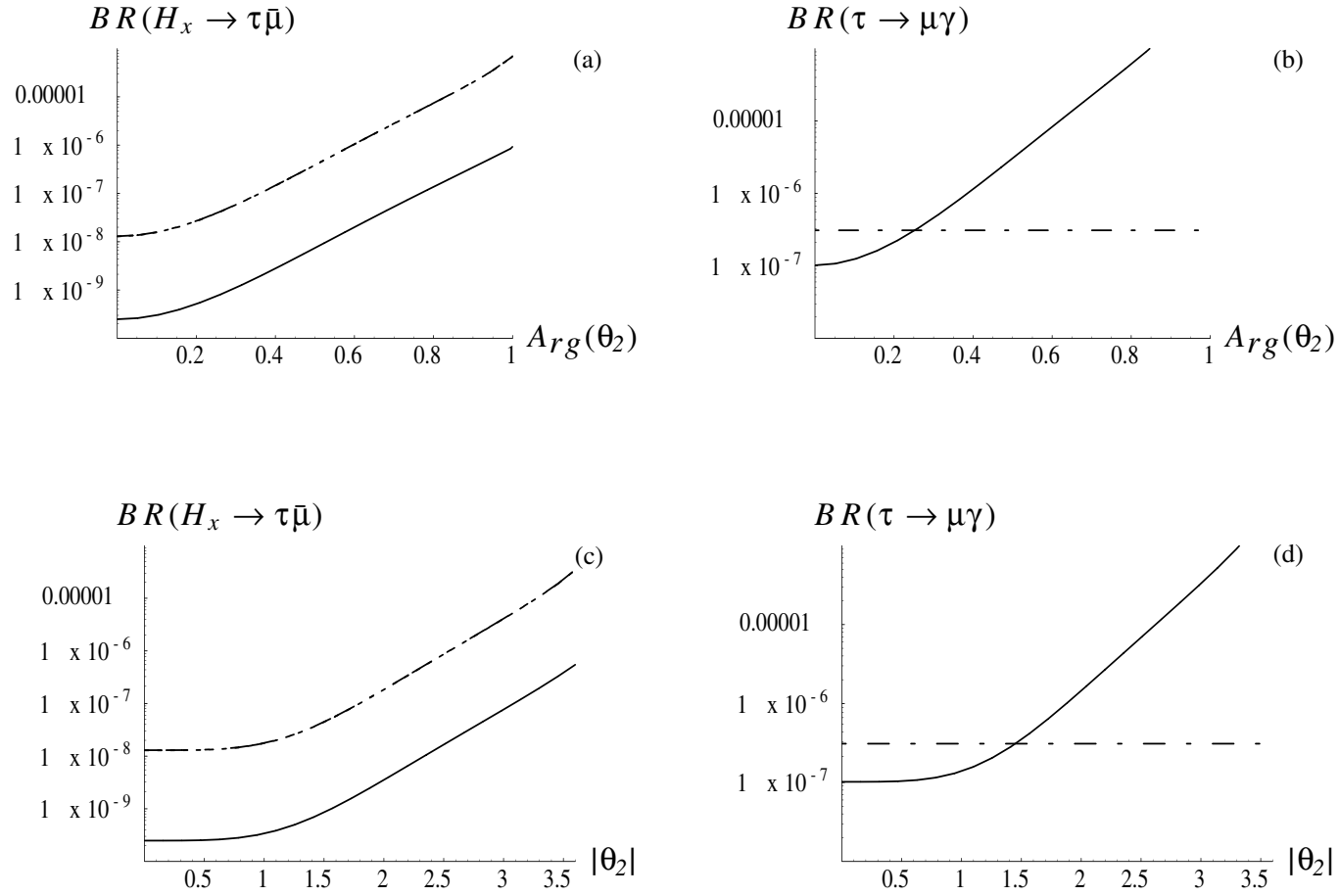

FIG. 8. (a) Dependence of BR($H_x \to \tau\bar{\mu}$) with Arg(θ_2) for $|\theta_2| = \pi$. (b) Dependence of BR($\tau \to \mu\gamma$) with Arg(θ_2) for $|\theta_2| = \pi$. (c) Dependence of BR($H_x \to \tau\bar{\mu}$) with $|\theta_2|$ for Arg(θ_2) $= \pi/4$. (d) Dependence of BR($\tau \to \mu\gamma$) with$|\theta_2|$ for Arg(θ_2) $= \pi/4$. All figures are in scenario B, case 1, for complex θ_2 and $\theta_1 = \theta_3 = 0$. The rest of the parameters are fixed to $(m_{N_1}, m_{N_2}, m_{N_3}) = (10^8, 2 \times 10^8, 10^{14})$ GeV, $\tan\beta = 50$, $M_0 = 400$ GeV, and $M_{1/2} = 300$ GeV. Solid, dashed, and dashed-dotted (the two latter undistinguishable here) lines in the left panels correspond to $H_x = (h_0, H_0, A_0)$, respectively. The horizontal line in the right panels is the experimental upper bound on $\tau \to \mu\gamma$.

within the experimentally allowed range. In summary, for real R we find that the maximum allowed LFVHD rates are at or below 1.3×10^{-8}.

The case of complex R is certainly more promising. The examples shown in Figs. 8(a) and 8(c) are for the most favorable case, among the ones studied here, of complex $\theta_2 \neq 0$ with $\theta_1 = \theta_3 = 0$. It shows that considerably larger BR($H_x \to \tau\bar{\mu}$) rates than in the real R case are found. For the explored θ_2 values in these plots, the Higgs rates grow with both $|\theta_2|$ and Arg(θ_2) and, for the selected values of the parameters in this figure, they reach values up to around 5×10^{-5}. We have checked that the predicted rates for BR($\tau \to e\gamma$) are well below the experimental upper bound and that the $\mu \to e\gamma$ decay is, in this case, less restrictive than the $\tau \to \mu\gamma$ decay. Notice that the smallness of the $\mu \to e\gamma$ and $\tau \to e\gamma$ decay rates, in the case under study of $\theta_2 \neq 0$, is not maintained if our hypothesis on $\theta_{13} = 0$ is changed. For instance, for $\theta_{13} = 5°$, which is also allowed by neutrino data, we get BR($\mu \to e\gamma$) $\sim 2.4 \times 10^{-8}$, for $\theta_2 = \pi e^{i(\pi/10)}$, well above the experimental upper bound. This is why we keep $\theta_{13} = 0$ in all this work. Therefore, in this case of complex $\theta_2 \neq 0$ with $\theta_{13} = 0$, the relevant lepton decay is $\tau \to \mu\gamma$ which is illustrated in Figs. 8(b) and 8(d) together with its experimental bound. We see that the allowed region by $\tau \to \mu\gamma$ data of the $[|\theta_2|, \text{Arg}(\theta_2)]$ parameter space implies a reduction in the Higgs rates, leading to a maximum allowed value of just 5×10^{-8}.

These results are for fixed values of $(m_{N_1}, m_{N_2}, m_{N_3}) = (10^8, 2 \times 10^8, 10^{14})$ GeV, $\tan\beta = 50$, $M_0 = 400$ GeV, and $M_{1/2} = 300$ GeV. We have found that other choices of the soft-SUSY-breaking mass parameters M_0 and $M_{1/2}$ are more efficient in order to get larger maximum allowed Higgs ratios. For instance, for $M_0 = M_{1/2} = 1200$ GeV, we find maximum allowed values of around 5.6×10^{-6}. The reason for this improvement is the different behavior with these parameters of the LFVHD and the lepton decay rates, which will be studied in more detail next.

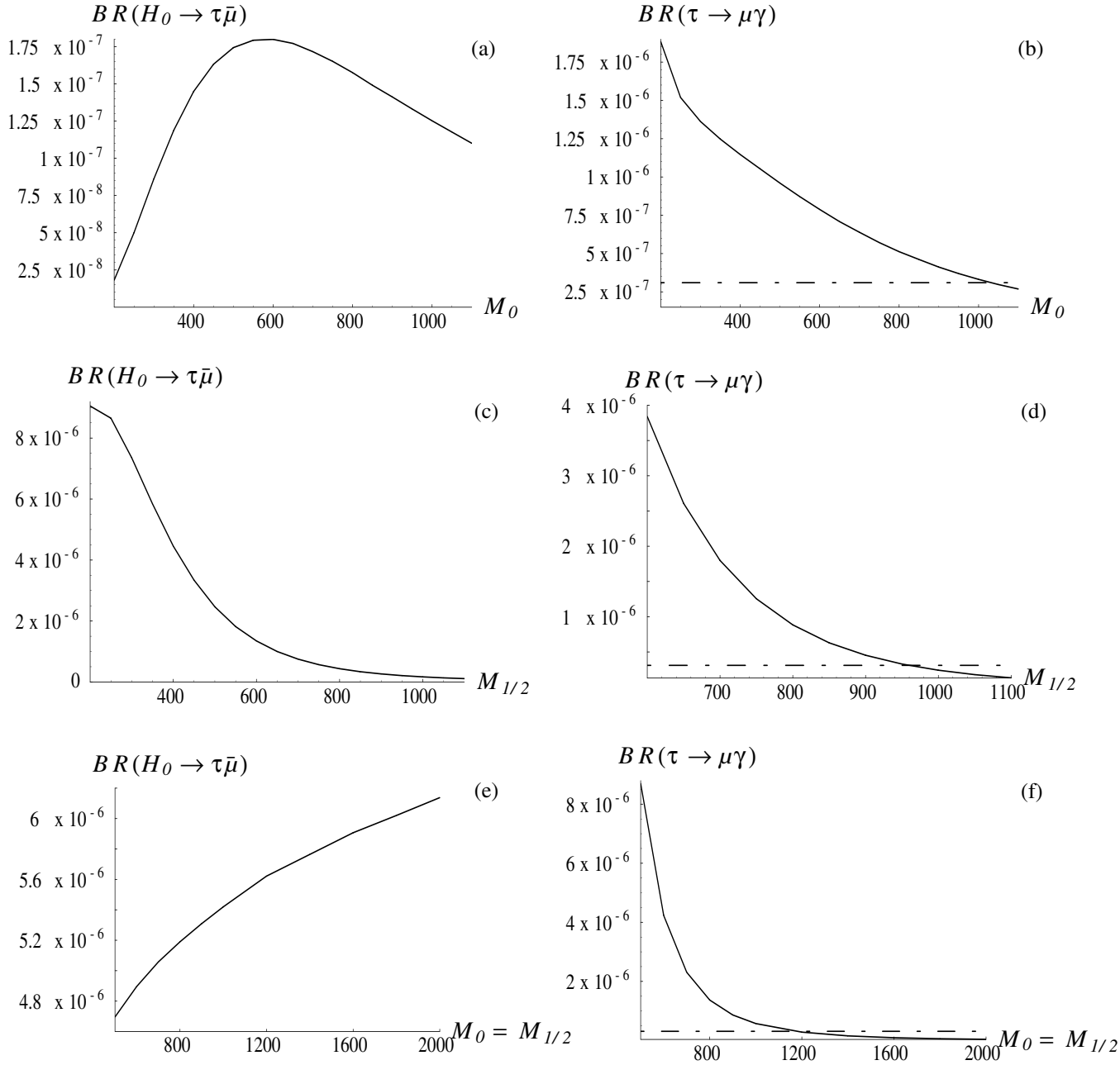

FIG. 9. Dependence with M_0 (GeV) and $M_{1/2}$ (GeV) for scenario B with $(m_{N_1}, m_{N_2}, m_{N_3}) = (10^8, 2 \times 10^8, 10^{14})$ GeV, $\theta_1 = \theta_3 = 0$, and $\tan\beta = 50$. (a) Behavior of BR($H_0 \to \tau\bar{\mu}$) with M_0 (GeV) for $M_{1/2} = 300$ GeV and $\theta_2 = \pi e^{0.4i}$. (b) Same as (a) but for BR($\tau \to \mu\gamma$). (c) Behavior of BR($H_0 \to \tau\bar{\mu}$) with $M_{1/2}$ (GeV) for $M_0 = 400$ GeV and $\theta_2 = \pi e^{0.8i}$. (d) Same as (c) but for BR($\tau \to \mu\gamma$). (e) Behavior of BR($H_0 \to \tau\bar{\mu}$) with $M_0 = M_{1/2}$ (GeV) for $\theta_2 = \pi e^{0.8i}$. (f) Same as (e) but for BR($\tau \to \mu\gamma$). The horizontal line in the right panels is the upper experimental bound on BR($\tau \to \mu\gamma$).

In Fig. 9 we show the dependence of BR($H^0 \to \tau\bar{\mu}$) and BR($\tau \to \mu\gamma$) with M_0 and $M_{1/2}$ for hierarchical neutrinos with $(m_{N_1}, m_{N_2}, m_{N_3}) = (10^8, 2 \times 10^8, 10^{14})$ GeV and fixed values of $\tan\beta = 50$, $\theta_2 \neq 0$, and $\theta_1 = \theta_3 = 0$. We see clearly in these plots the different behavior of these two observables with the soft-SUSY-breaking mass parameters. Figures 9(a) and 9(c) show a milder dependence of BR($H^0 \to \tau\bar{\mu}$) on M_0 and $M_{1/2}$ than that of BR($\tau \to \mu\gamma$) in Figs. 9(b) and 9(d), respectively. This implies that, for large enough values of M_0 or $M_{1/2}$ or both, the BR($\tau \to \mu\gamma$) rates get considerably suppressed, due to the decoupling of the heavy SUSY particles in the loops, and enter into the allowed region by data, whereas the BR($H^0 \to \tau\bar{\mu}$) rates are not much reduced. In fact, we see in Figs. 9(e) and 9(f) that for the choice $M_0 = M_{1/2}$ the tau decay ratio crosses down the upper experimental bound at around

$M_0 = 1200$ GeV, whereas the Higgs decay ratio is still quite large $\sim 6 \times 10^{-6}$ in the high M_0 region, around $M_0 \simeq 2000$ GeV. This behavior with the soft-SUSY-breaking parameters is a clear indication that the heavy SUSY particles in the loops do not decouple in the LFVHD, in much the same way as it has been shown to happen in the case of Higgs decays into quarks with change of flavor [4]. Notice that the nondecoupling of the SUSY particles in the LFVHD can also be reformulated as nondecoupling in the effective $H^{(x)}\tau\mu$ couplings and these in turn can induce large contributions to other LFV processes that are mediated by Higgs exchange as, for instance, $\tau \to \mu\mu\mu$ [25]. However, we have checked that for the explored values in this work of M_0, $M_{1/2}$, $\tan\beta$, R, and m_{N_i} that lead to the announced LFVHD ratios of about 6×10^{-6}, the corresponding $\mathrm{BR}(\tau \to \mu\mu\mu)$ rates are below the present experimental upper bound of 2×10^{-7} [26].

Finally, in order to show more clearly the nondecoupling behavior of the SUSY particles in the contributing loops to the LFVHD we consider, instead of mSUGRA, a simpler and more generic MSSM scenario, with the λ_{ij} being free parameters, which we now fix to some particular values, concretely, $\lambda_{23} = -0.4$ and $\lambda_{12} = \lambda_{13} = 0$. For simplicity, we also assume a common SUSY mass at the electroweak scale, $M_{\mathrm{SUSY}} \equiv m_{\tilde{L},l} = m_{\tilde{E},l} = M_0 = \mu$ and choose $M_2 = \frac{2}{3}\mu$, $M_1 = \frac{5}{3}\tan^2\theta_W M_2$. This particular value of λ_{23} corresponds roughly to the predicted λ_{23} in the MSSM-seesaw with the parameters set in Fig. 9(e). Finally, the $\mathrm{BR}(H_0 \to \tau\bar{\mu})$ is shown in Fig. 10 as a function of this common M_{SUSY} scale, for $\tan\beta = 50$ and $m_{H_0} = 340$ GeV. We see clearly that for large M_{SUSY} the branching ratio approaches a constant nonvanishing value, which for these input parameter values is of about 10^{-5}, and therefore the charginos, neutralinos, charged sleptons, and sneutrinos do not decouple in this observable. Another way of seeing this explicitly is by the analytical computation of this observable in the large SUSY masses limit. We have performed this computation in the simplest case where all the SUSY masses are equal and got the following asymptotic limits for the dominant form factor F_L, in the regime of small λ_{23} and large $\tan\beta$:

$$F_{L\chi^{\pm}}^{(H^0)} = -\frac{\alpha}{4\pi\sin^2\theta_W}\frac{m_\tau}{12 m_W}\lambda_{23}(\tan\beta)^2, \tag{37}$$

$$F_{L\chi^{0}}^{(H^0)} = -\frac{\alpha}{4\pi\sin^2\theta_W}\frac{m_\tau}{24 m_W}(1 - 3\tan^2\theta_W)\lambda_{23}(\tan\beta)^2. \tag{38}$$

From these simple expressions we can estimate quite easily the LFVHD ratios. For instance, for the parameters chosen in Fig. 10, we get $\mathrm{BR}(H^0 \to \tau\bar{\mu}) \simeq 3 \times 10^{-6}$ in reasonable agreement with our numerical result in this figure and in Fig. 9(e). Notice also that this asymptotic result agrees with the result from the effective Lagrangian approach in Ref. [15]. Finally, it is worth mentioning that this nondecoupling behavior is in contrast with the behavior of $\mathrm{BR}(\mu \to e\gamma)$, which scales as $(M_W/M_{\mathrm{SUSY}})^4$, and explains the comparatively large LFVHD rates found here.

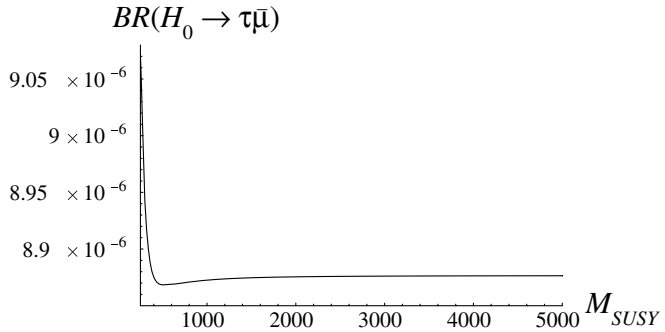

FIG. 10. Behavior of $H_0 \to \tau\bar{\mu}$ in a generic MSSM scenario as a function of the common SUSY mass, M_{SUSY} (GeV) $\equiv m_{\tilde{L},l} = m_{\tilde{E},l} = M_0 = \mu$. The gaugino soft masses are set to $M_2 = 2/3\mu$ and $M_1 = \frac{5}{3}\tan^2\theta_W M_2$. Here we fix $\lambda_{23} = -0.4$, $\lambda_{12} = \lambda_{13} = 0$, $\tan\beta = 50$, and $m_{H_0} = 340$ GeV.

V. CONCLUSIONS

In this paper, we have studied in full detail the lepton flavor violating Higgs boson decays that are produced if the neutrinos get their masses via the seesaw mechanism. We have considered the two most popular seesaw models with three generations, the SM-seesaw and the MSSM-seesaw. Within the SM-seesaw we have found extremely small branching ratios which are explained in terms of the decoupling behavior of the heavy Majorana neutrinos and the smallness of the light neutrino masses. In the MSSM-seesaw we find, in contrast, branching ratios that are many orders of magnitude larger. The larger ratios found are for $H_0 \to \tau\bar{\mu}$ and $A_0 \to \tau\bar{\mu}$ decays with similar rates. After exploring the dependence of the $H_0 \to \tau\bar{\mu}$ decay rates with all the involved parameters of the MSSM-seesaw and by requiring compatibility with data of the correlated predictions for $\mu \to e\gamma$, $\tau \to e\gamma$, and $\tau \to \mu\gamma$ decays, we find that $\mathrm{BR}(H_0 \to \tau\bar{\mu})$ as large as 10^{-5} for hierarchical neutrinos and large M_{SUSY} can be reached. These ratios are mostly sensitive to $\tan\beta$, the heaviest neutrino mass m_{N_3}, and the complex angle θ_2, which have been taken in the range $3 < \tan\beta < 50$, 10^8 GeV $< m_{N_3} < 10^{14}$ GeV, and $[|\theta_2|, \mathrm{Arg}(\theta_2)] \leq (3.5, 1)$, respectively. The largest allowed ratios found in this work of about 10^{-5} are for $\tan\beta = 50$, $m_{N_3} = 10^{14}$ GeV, large M_{SUSY} in the TeV range, and for our choice of $\theta_2 = \pi e^{0.8i}$, $\theta_1 = \theta_3 = 0$, but a more refined analysis of the full parameter space could lead to even larger rates. In particular, it is obvious that larger $\tan\beta$ values will enhance considerably the rates and lead to Higgs ratios closer to the future experimental reach of 10^{-4} at LHC [27] and e^+e^- and $\mu^+\mu^-$ colliders [28], but we have not tried this because it would require performing a resummation of the large $\tan\beta$ contributions that is beyond the scope of this work.

ACKNOWLEDGMENTS

We are indebted to Alberto Casas and Alejandro Ibarra for valuable discussions and for helping us in the estimate of the RGE-running effects on the neutrino masses and mixings. We acknowledge Andrea Brignole and Anna Rossi for warning us of an error in the previous version of this work. We also thank Ana Teixeira for her help with the usage of the MSUSPECT package. We appreciate the updated information on LFV data that was provided to us by Eric Torrence. D. T. thanks F. Boudjema for useful comments and for reading the manuscript. E. A. and A. M. C. acknowledge the Spanish Ministry of Science and Education (MEC) for financial support by their FPU Grants, No. AP2003-3776 and No. AP2001-0678, respectively. This work was supported by the Spanish MEC under Project No. FPA2003-04597.

APPENDIX A

We present here the analytical results for the form factors in the SM-seesaw, in the Feynman 't Hooft gauge.

$$
\begin{aligned}
F_L^{(1)} &= -\frac{g^2}{4m_W^3}\frac{1}{16\pi^2}B_{l_k n_i}B^*_{l_m n_j}\{m_{l_k}m_{n_j}[(m_{n_i}+m_{n_j})\mathrm{Re}(C_{n_i n_j})+i(m_{n_j}-m_{n_i})\mathrm{Im}(C_{n_i n_j})]\tilde{C}_0+(C_{12}-C_{11})\\
&\quad\times[(m_{n_i}+m_{n_j})\mathrm{Re}(C_{n_i n_j})(-m_{l_k}^3m_{n_j}-m_{n_i}m_{l_k}m_{l_m}^2+m_{n_i}m_{n_j}^2m_{l_k}+m_{n_i}^2m_{n_j}m_{l_k})+i(m_{n_j}-m_{n_i})\mathrm{Im}(C_{n_i n_j})\\
&\quad\times(-m_{l_k}^3m_{n_j}+m_{n_i}m_{l_k}m_{l_m}^2-m_{n_i}m_{n_j}^2m_{l_k}+m_{n_i}^2m_{n_j}m_{l_k})]\},\\
F_R^{(1)} &= \frac{g^2}{4m_W^3}\frac{1}{16\pi^2}B_{l_k n_i}B^*_{l_m n_j}\{m_{n_i}m_{l_m}[(m_{n_i}+m_{n_j})\mathrm{Re}(C_{n_i n_j})-i(m_{n_j}-m_{n_i})\mathrm{Im}(C_{n_i n_j})]\tilde{C}_0+C_{12}[(m_{n_i}+m_{n_j})\\
&\quad\times\mathrm{Re}(C_{n_i n_j})(m_{l_m}^3m_{n_i}-m_{n_i}m_{n_j}^2m_{l_m}-m_{n_i}^2m_{n_j}m_{l_m}+m_{n_j}m_{l_k}^2m_{l_m})+i(m_{n_j}-m_{n_i})\mathrm{Im}(C_{n_i n_j})\\
&\quad\times(-m_{l_m}^3m_{n_i}+m_{n_i}m_{n_j}^2m_{l_m}-m_{n_i}^2m_{n_j}m_{l_m}+m_{n_j}m_{l_k}^2m_{l_m})]\},
\end{aligned}
$$

where $C_{11,12}=C_{11,12}(m_{l_k}^2,m_H^2,m_W^2,m_{n_i}^2,m_{n_j}^2)$ and $\tilde{C}_0=\tilde{C}_0(m_{l_k}^2,m_H^2,m_W^2,m_{n_i}^2,m_{n_j}^2)$.

$$
\begin{aligned}
F_L^{(2)} &= \frac{g^2}{2m_W}\frac{1}{16\pi^2}B_{l_k n_i}B^*_{l_m n_j}m_{l_k}\{-m_{n_j}[(m_{n_i}+m_{n_j})\mathrm{Re}(C_{n_i n_j})+i(m_{n_j}-m_{n_i})\mathrm{Im}(C_{n_i n_j})]C_0+(C_{12}-C_{11})\\
&\quad\times[(m_{n_i}+m_{n_j})^2\mathrm{Re}(C_{n_i n_j})+i(m_{n_j}-m_{n_i})^2\mathrm{Im}(C_{n_i n_j})]\},\\
F_R^{(2)} &= -\frac{g^2}{2m_W}\frac{1}{16\pi^2}B_{l_k n_i}B^*_{l_m n_j}m_{l_m}\{m_{n_i}[(m_{n_i}+m_{n_j})\mathrm{Re}(C_{n_i n_j})-i(m_{n_j}-m_{n_i})\mathrm{Im}(C_{n_i n_j})]C_0+C_{12}[(m_{n_i}+m_{n_j})^2\\
&\quad\times\mathrm{Re}(C_{n_i n_j})+i(m_{n_j}-m_{n_i})^2\mathrm{Im}(C_{n_i n_j})]\},
\end{aligned}
$$

where $C_{0,11,12}=C_{0,11,12}(m_{l_k}^2,m_H^2,m_W^2,m_{n_i}^2,m_{n_j}^2)$.

$$
F_L^{(3)}=\frac{g^2}{16\pi^2}B_{l_k n_i}B^*_{l_m n_i}m_{l_k}m_W(C_{11}-C_{12}),\qquad F_R^{(3)}=\frac{g^2}{16\pi^2}B_{l_k n_i}B^*_{l_m n_i}m_{l_m}m_WC_{12},
$$

where $C_{11,12}=C_{11,12}(m_{l_k}^2,m_H^2,m_{n_i}^2,m_W^2,m_W^2)$.

$$
\begin{aligned}
F_L^{(4)} &= -\frac{g^2}{4m_W}\frac{1}{16\pi^2}B_{l_k n_i}B^*_{l_m n_i}m_{l_k}\{m_{l_m}^2(C_{12}-2C_{11})+m_{n_i}^2(C_{11}-C_{12})-m_{n_i}^2C_0\},\\
F_R^{(4)} &= -\frac{g^2}{4m_W}\frac{1}{16\pi^2}B_{l_k n_i}B^*_{l_m n_i}m_{l_m}\{\tilde{C}_0+2m_{l_m}^2C_{11}+m_{n_i}^2C_{12}+(m_{l_k}^2-2m_H^2)(C_{11}-C_{12})+2m_{n_i}^2C_0\},
\end{aligned}
$$

where $C_{0,11,12}=C_{0,11,12}(m_{l_k}^2,m_H^2,m_{n_i}^2,m_W^2,m_W^2)$ and $\tilde{C}_0=\tilde{C}_0(m_{l_k}^2,m_H^2,m_{n_i}^2,m_W^2,m_W^2)$.

$$
\begin{aligned}
F_L^{(5)} &= -\frac{g^2}{4m_W}\frac{1}{16\pi^2}B_{l_k n_i}B^*_{l_m n_i}m_{l_k}\{\tilde{C}_0+2m_{n_i}^2C_0+(m_{n_i}^2+2m_{l_k}^2)C_{11}+(m_{l_m}^2-m_{n_i}^2-2m_H^2)C_{12}\},\\
F_R^{(5)} &= \frac{g^2}{4m_W}\frac{1}{16\pi^2}B_{l_k n_i}B^*_{l_m n_i}m_{l_m}\{m_{n_i}^2C_0+m_{l_k}^2C_{11}+(m_{l_k}^2-m_{n_i}^2)C_{12}\},
\end{aligned}
$$

where $C_{0,11,12}=C_{0,11,12}(m_{l_k}^2,m_H^2,m_{n_i}^2,m_W^2,m_W^2)$ and $\tilde{C}_0=\tilde{C}_0(m_{l_k}^2,m_H^2,m_{n_i}^2,m_W^2,m_W^2)$.

$$F_L^{(6)} = \frac{g^2}{4m_W^3}\frac{1}{16\pi^2} B_{l_k n_i} B^*_{l_m n_i} m_{l_k} m_H^2 \{m_{n_i}^2 (C_0 + C_{11}) + (m_{l_m}^2 - m_{n_i}^2) C_{12}\},$$

$$F_R^{(6)} = \frac{g^2}{4m_W^3}\frac{1}{16\pi^2} B_{l_k n_i} B^*_{l_m n_i} m_{l_m} m_H^2 \{m_{n_i}^2 (C_0 + C_{12}) + m_{l_k}^2 (C_{11} - C_{12})\},$$

where $C_{0,11,12} = C_{0,11,12}(m_{l_k}^2, m_H^2, m_{n_i}^2, m_W^2, m_W^2)$.

$$F_L^{(7)} = \frac{g^2}{2m_W}\frac{1}{16\pi^2} B_{l_k n_i} B^*_{l_m n_i} \frac{m_{l_m}^2 m_{l_k}}{m_{l_k}^2 - m_{l_m}^2} B_1, \qquad F_R^{(7)} = \frac{g^2}{2m_W}\frac{1}{16\pi^2} B_{l_k n_i} B^*_{l_m n_i} \frac{m_{l_k}^2 m_{l_m}}{m_{l_k}^2 - m_{l_m}^2} B_1,$$

$$F_L^{(8)} = \frac{g^2}{4m_W^3}\frac{1}{16\pi^2} B_{l_k n_i} B^*_{l_m n_i} \frac{m_{l_k}}{m_{l_k}^2 - m_{l_m}^2} \{m_{l_m}^2 (m_{l_k}^2 + m_{n_i}^2) B_1 + 2 m_{n_i}^2 m_{l_m}^2 B_0\},$$

$$F_R^{(8)} = \frac{g^2}{4m_W^3}\frac{1}{16\pi^2} B_{l_k n_i} B^*_{l_m n_i} \frac{m_{l_m}}{m_{l_k}^2 - m_{l_m}^2} \{m_{l_k}^2 (m_{l_m}^2 + m_{n_i}^2) B_1 + m_{n_i}^2 (m_{l_k}^2 + m_{l_m}^2) B_0\},$$

where $B_{0,1} = B_{0,1}(m_{l_k}^2, m_{n_i}^2, m_W^2)$.

$$F_L^{(9)} = \frac{g^2}{2m_W}\frac{1}{16\pi^2} B_{l_k n_i} B^*_{l_m n_i} \frac{m_{l_m}^2 m_{l_k}}{m_{l_m}^2 - m_{l_k}^2} B_1, \qquad F_R^{(9)} = \frac{g^2}{2m_W}\frac{1}{16\pi^2} B_{l_k n_i} B^*_{l_m n_i} \frac{m_{l_k}^2 m_{l_m}}{m_{l_m}^2 - m_{l_k}^2} B_1,$$

$$F_L^{(10)} = \frac{g^2}{4m_W^3}\frac{1}{16\pi^2} B_{l_k n_i} B^*_{l_m n_i} \frac{m_{l_k}}{m_{l_m}^2 - m_{l_k}^2} \{m_{l_m}^2 (m_{l_k}^2 + m_{n_i}^2) B_1 + m_{n_i}^2 (m_{l_k}^2 + m_{l_m}^2) B_0\},$$

$$F_R^{(10)} = \frac{g^2}{4m_W^3}\frac{1}{16\pi^2} B_{l_k n_i} B^*_{l_m n_i} \frac{m_{l_m}}{m_{l_m}^2 - m_{l_k}^2} \{m_{l_k}^2 (m_{l_m}^2 + m_{n_i}^2) B_1 + 2 m_{n_i}^2 m_{l_k}^2 B_0\},$$

where $B_{0,1} = B_{0,1}(m_{l_m}^2, m_{n_i}^2, m_W^2)$.

$$\tilde{C}_0(p_2^2, p_1^2, m_1^2, m_2^2, m_3^2) \equiv B_0(p_1^2, m_2^2, m_3^2) + m_1^2 C_0(p_2^2, p_1^2, m_1^2, m_2^2, m_3^2).$$

In all the previous formulas, summation over all indices are understood. These run as $i, j = 1, \ldots 6$ for neutrinos and $k, m = 1, \ldots 3$, for charged leptons.

APPENDIX B

1. Couplings in the MSSM-seesaw

We present here the coupling factors entering in the MSSM-seesaw formulas.

$$A^{(e,\mu,\tau)}_{L\alpha j} = -\frac{m_{e,\mu,\tau}}{\sqrt{2}m_W\cos\beta}U^*_{j2}R^{(\nu)}_{(1,2,3)\alpha}, \qquad A^{(e,\mu,\tau)}_{R\alpha j} = V_{j1}R^{(\nu)}_{(1,2,3)\alpha},$$

$$B^{(e,\mu,\tau)}_{L\alpha a} = \sqrt{2}\left[\frac{m_{e,\mu,\tau}}{2m_W\cos\beta}N^*_{a3}R^{(l)}_{(1,3,5)\alpha} + \left(\sin\theta_W N'^*_{a1} - \frac{\sin^2\theta_W}{\cos\theta_W}N'^*_{a2}\right)R^{(l)}_{(2,4,6)\alpha}\right],$$

$$B^{(e,\mu,\tau)}_{R\alpha a} = \sqrt{2}\left\{\left[-\sin\theta_W N'_{a1} - \frac{1}{\cos\theta_W}\left(\frac{1}{2} - \sin^2\theta_W\right)N'_{a2}\right]R^{(l)}_{(1,3,5)\alpha} + \frac{m_{e,\mu,\tau}}{2m_W\cos\beta}N_{a3}R^{(l)}_{(2,4,6)\alpha}\right\},$$

$$W^{(x)}_{Lij} = \frac{1}{\sqrt{2}}(-\sigma^{(x)}_1 U^*_{j2}V^*_{i1} + \sigma^{(x)}_2 U^*_{j1}V^*_{i2}); \qquad W^{(x)}_{Rij} = \frac{1}{\sqrt{2}}(-\sigma^{(x)}_1 U_{i2}V_{j1} + \sigma^{(x)}_2 U_{i1}V_{j2}),$$

$$D^{(x)}_{Lab} = \frac{1}{2\cos\theta_W}[(\sin\theta_W N^*_{b1} - \cos\theta_W N^*_{b2})(\sigma^{(x)}_1 N^*_{a3} + \sigma^{(x)}_2 N^*_{a4}) + (\sin\theta_W N^*_{a1} - \cos\theta_W N^*_{a2})(\sigma^{(x)}_1 N^*_{b3} + \sigma^{(x)}_2 N^*_{b4})];$$

$$D^{(x)}_{Rab} = D^{(x)*}_{Lab}, \qquad S^{(x)}_{L,l} = -\frac{m_l}{2m_W\cos\beta}\sigma^{(x)*}_1;$$

$$S^{(x)}_{R,l} = S^{(x)*}_{L,l},$$

$$g_{H_x\tilde{l}_\alpha\tilde{l}_\beta} = -ig[g^{(x)}_{LL,e}R^{*(l)}_{1\alpha}R^{(l)}_{1\beta} + g^{(x)}_{RR,e}R^{*(l)}_{2\alpha}R^{(l)}_{2\beta} + g^{(x)}_{LR,e}R^{*(l)}_{1\alpha}R^{(l)}_{2\beta} + g^{(x)}_{RL,e}R^{*(l)}_{2\alpha}R^{(l)}_{1\beta} + g^{(x)}_{LL,\mu}R^{*(l)}_{3\alpha}R^{(l)}_{3\beta} + g^{(x)}_{RR,\mu}R^{*(l)}_{4\alpha}R^{(l)}_{4\beta}$$
$$+ g^{(x)}_{LR,\mu}R^{*(l)}_{3\alpha}R^{(l)}_{4\beta} + g^{(x)}_{RL,\mu}R^{*(l)}_{4\alpha}R^{(l)}_{3\beta} + g^{(x)}_{LL,\tau}R^{*(l)}_{5\alpha}R^{(l)}_{5\beta} + g^{(x)}_{RR,\tau}R^{*(l)}_{6\alpha}R^{(l)}_{6\beta} + g^{(x)}_{LR,\tau}R^{*(l)}_{5\alpha}R^{(l)}_{6\beta} + g^{(x)}_{RL,\tau}R^{*(l)}_{6\alpha}R^{(l)}_{5\beta}],$$

$$g_{H_x\tilde{\nu}_\alpha\tilde{\nu}_\beta} = -ig[g^{(x)}_{LL,\nu}R^{*(\nu)}_{1\alpha}R^{(\nu)}_{1\beta} + g^{(x)}_{LL,\nu}R^{*(\nu)}_{2\alpha}R^{(\nu)}_{2\beta} + g^{(x)}_{LL,\nu}R^{*(\nu)}_{3\alpha}R^{(\nu)}_{3\beta}],$$

$$g^{(x)}_{LL,l} = \frac{M_Z}{\cos\theta_W}\sigma^{(x)}_3\left(\frac{1}{2} - \sin^2\theta_W\right) + \frac{m^2_l}{M_W\cos\beta}\sigma^{(x)}_4,$$

$$g^{(x)}_{RR,l} = \frac{M_Z}{\cos\theta_W}\sigma^{(x)}_3(\sin^2\theta_W) + \frac{m^2_l}{M_W\cos\beta}\sigma^{(x)}_4, \qquad g^{(x)}_{LR,l} = (-\sigma^{(x)}_1 A_l - \sigma^{(x)}_5\mu)\frac{m_l}{2M_W\cos\beta}; \qquad g^{(x)}_{RL,l} = g^{(x)*}_{LR,l},$$

$$g^{(x)}_{LL,\nu} = -\frac{M_Z}{2\cos\theta_W}\sigma^{(x)}_3,$$

where

$$\sigma^{(x)}_1 = \begin{pmatrix}\sin\alpha\\ -\cos\alpha\\ i\sin\beta\end{pmatrix}, \qquad \sigma^{(x)}_2 = \begin{pmatrix}\cos\alpha\\ \sin\alpha\\ -i\cos\beta\end{pmatrix}, \qquad \sigma^{(x)}_3 = \begin{bmatrix}\sin(\alpha+\beta)\\ -\cos(\alpha+\beta)\\ 0\end{bmatrix}$$

and

$$\sigma^{(x)}_4 = \begin{pmatrix}-\sin\alpha\\ \cos\alpha\\ 0\end{pmatrix}, \qquad \sigma^{(x)}_5 = \begin{pmatrix}\cos\alpha\\ \sin\alpha\\ i\cos\beta\end{pmatrix}, \qquad \text{for} \quad x = \begin{pmatrix}h^0\\ H^0\\ A^0\end{pmatrix},$$

respectively. The matrices that rotate to the mass eigenstate basis are U and V for charginos, N for neutralinos, $R^{(l)}$ for charged sleptons, and $R^{(\nu)}$ for sneutrinos. U, V, and N are taken from Ref. [29], $N'_{a1} = N_{a1}\cos\theta_W + N_{a2}\sin\theta_W$, $N'_{a2} = -N_{a1}\sin\theta_W + N_{a2}\cos\theta_W$, and $R^{(l)}$ and $R^{(\nu)}$ are computed here by the diagonalization procedure presented in Sec. IV. The various indices in the previous formulas run as follows: $i, j = 1, 2$ for charginos, $a, b = 1, \ldots, 4$ for neutralinos, $\alpha, \beta = 1, \ldots, 6$ for charged sleptons, $\alpha, \beta = 1, \ldots, 3$ for sneutrinos, and $l = e, \mu, \tau$ for charged leptons. Summation over all indices is understood.

2. Form factors in the MSSM-seesaw

We present here the analytical results for the form factors in the MSSM-seesaw.

$$F^{(1)}_{L,x} = -\frac{g^2}{16\pi^2}\{[B_0 + m^2_{\tilde{\nu}_\alpha} C_0 + m^2_{l_m} C_{12} + m^2_{l_k}(C_{11} - C_{12})]\kappa^{x,\tilde{\chi}^-}_{L1} + m_{l_k} m_{l_m}(C_{11} + C_0)\kappa^{x,\tilde{\chi}^-}_{L2} + m_{l_k} m_{\tilde{\chi}^-_j}(C_{11} - C_{12} + C_0)\kappa^{x,\tilde{\chi}^-}_{L3} + m_{l_m} m_{\tilde{\chi}^-_j} C_{12}\kappa^{x,\tilde{\chi}^-}_{L4} + m_{l_k} m_{\tilde{\chi}^-_i}(C_{11} - C_{12})\kappa^{x,\tilde{\chi}^-}_{L5} + m_{l_m} m_{\tilde{\chi}^-_i}(C_{12} + C_0)\kappa^{x,\tilde{\chi}^-}_{L6} + m_{\tilde{\chi}^-_i} m_{\tilde{\chi}^-_j} C_0 \kappa^{x,\tilde{\chi}^-}_{L7}\},$$

$$F^{(2)}_{L,x} = -\frac{igg_{H_x\tilde{\nu}_\alpha\tilde{\nu}_\beta}}{16\pi^2}[-m_{l_k}(C_{11} - C_{12})\iota^{x,\tilde{\chi}^-}_{L1} - m_{l_m} C_{12}\iota^{x,\tilde{\chi}^-}_{L2} + m_{\tilde{\chi}^-_i} C_0 \iota^{x,\tilde{\chi}^-}_{L3}],$$

$$F^{(3)}_{L,x} = -\frac{S^{(x)}_{L,l_m}}{m^2_{l_k} - m^2_{l_m}}\{m^2_{l_k}\Sigma^{\tilde{\chi}^-}_R(m^2_{l_k}) + m^2_{l_k}\Sigma^{\tilde{\chi}^-}_{Rs}(m^2_{l_k}) + m_{l_m}[m_{l_k}\Sigma^{\tilde{\chi}^-}_L(m^2_{l_k}) + m_{l_k}\Sigma^{\tilde{\chi}^-}_{Ls}(m^2_{l_k})]\},$$

$$F^{(4)}_{L,x} = -\frac{S^{(x)}_{L,l_k}}{m^2_{l_m} - m^2_{l_k}}\{m^2_{l_m}\Sigma^{\tilde{\chi}^-}_L(m^2_{l_m}) + m_{l_m} m_{l_k}\Sigma^{\tilde{\chi}^-}_{Rs}(m^2_{l_m}) + m_{l_k}[m_{l_m}\Sigma^{\tilde{\chi}^-}_R(m^2_{l_m}) + m_{l_k}\Sigma^{\tilde{\chi}^-}_{Ls}(m^2_{l_m})]\},$$

$$F^{(5)}_{L,x} = -\frac{g^2}{16\pi^2}\{[B_0 + m^2_{\tilde{l}_\alpha} C_0 + m^2_{l_m} C_{12} + m^2_{l_k}(C_{11} - C_{12})]\kappa^{x,\tilde{\chi}^0}_{L1} + m_{l_k} m_{l_m}(C_{11} + C_0)\kappa^{x,\tilde{\chi}^0}_{L2} + m_{l_k} m_{\tilde{\chi}^0_b}(C_{11} - C_{12} + C_0)\kappa^{x,\tilde{\chi}^0}_{L3} + m_{l_m} m_{\tilde{\chi}^0_b} C_{12}\kappa^{x,\tilde{\chi}^0}_{L4} + m_{l_k} m_{\tilde{\chi}^0_a}(C_{11} - C_{12})\kappa^{x,\tilde{\chi}^0}_{L5} + m_{l_m} m_{\tilde{\chi}^0_a}(C_{12} + C_0)\kappa^{x,\tilde{\chi}^0}_{L6} + m_{\tilde{\chi}^0_a} m_{\tilde{\chi}^0_b} C_0 \kappa^{x,\tilde{\chi}^0}_{L7}\},$$

$$F^{(6)}_{L,x} = -\frac{igg_{H_x\tilde{l}_\alpha\tilde{l}_\beta}}{16\pi^2}[-m_{l_k}(C_{11} - C_{12})\iota^{x,\tilde{\chi}^0}_{L1} - m_{l_m} C_{12}\iota^{x,\tilde{\chi}^0}_{L2} + m_{\tilde{\chi}^0_a} C_0 \iota^{x,\tilde{\chi}^0}_{L3}],$$

$$F^{(7)}_{L,x} = -\frac{S^{(x)}_{L,l_m}}{m^2_{l_k} - m^2_{l_m}}\{m^2_{l_k}\Sigma^{\tilde{\chi}^0}_R(m^2_{l_k}) + m^2_{l_k}\Sigma^{\tilde{\chi}^0}_{Rs}(m^2_{l_k}) + m_{l_m}[m_{l_k}\Sigma^{\tilde{\chi}^0}_L(m^2_{l_k}) + m_{l_k}\Sigma^{\tilde{\chi}^0}_{Ls}(m^2_{l_k})]\},$$

$$F^{(8)}_{L,x} = -\frac{S^{(x)}_{L,l_k}}{m^2_{l_m} - m^2_{l_k}}\{m^2_{l_m}\Sigma^{\tilde{\chi}^0}_L(m^2_{l_m}) + m_{l_m} m_{l_k}\Sigma^{\tilde{\chi}^0}_{Rs}(m^2_{l_m}) + m_{l_k}[m_{l_m}\Sigma^{\tilde{\chi}^0}_R(m^2_{l_m}) + m_{l_k}\Sigma^{\tilde{\chi}^0}_{Ls}(m^2_{l_m})]\},$$

where

$$C_{0,11,12} = \begin{cases} C_{0,11,12}(m^2_{l_k}, m^2_{H_x}, m^2_{\tilde{\nu}_\alpha}, m^2_{\tilde{\chi}^-_i}, m^2_{\tilde{\chi}^-_j}) & \text{in } F^{(1)}_{L,x} \\ C_{0,11,12}(m^2_{l_k}, m^2_{H_x}, m^2_{\tilde{\chi}^-_i}, m^2_{\tilde{\nu}_\alpha}, m^2_{\tilde{\nu}_\beta}) & \text{in } F^{(2)}_{L,x} \\ C_{0,11,12}(m^2_{l_k}, m^2_{H_x}, m^2_{\tilde{l}_\alpha}, m^2_{\tilde{\chi}^0_a}, m^2_{\tilde{\chi}^0_b}) & \text{in } F^{(5)}_{L,x} \\ C_{0,11,12}(m^2_{l_k}, m^2_{H_x}, m^2_{\tilde{\chi}^0_a}, m^2_{\tilde{l}_\alpha}, m^2_{\tilde{l}_\beta}) & \text{in } F^{(6)}_{L,x} \end{cases}$$

and

$$\Sigma^{\tilde{\chi}}(k) = k\Sigma^{\tilde{\chi}}_L(k^2)P_L + k\Sigma^{\tilde{\chi}}_R(k^2)P_R + m[\Sigma^{\tilde{\chi}}_{Ls}(k^2)P_L + \Sigma^{\tilde{\chi}}_{Rs}(k^2)P_R]. \tag{B1}$$

The coupling factors and self-energies appearing in the neutralino contributions to the form factors are given by

$$\begin{aligned}
\kappa^{x,\tilde{\chi}^0}_{L1} &= B^{(l_k)}_{L\alpha a} D^{(x)}_{Rab} B^{(l_m)*}_{R\alpha b}, & \iota^{x,\tilde{\chi}^0}_{L1} &= B^{(l_k)}_{R\alpha a} B^{(l_m)*}_{R\beta a}, \\
\kappa^{x,\tilde{\chi}^0}_{L2} &= B^{(l_k)}_{R\alpha a} D^{(x)}_{Lab} B^{(l_m)*}_{L\alpha b}, & \iota^{x,\tilde{\chi}^0}_{L2} &= B^{(l_k)}_{L\alpha a} B^{(l_m)*}_{L\beta a}, \\
\kappa^{x,\tilde{\chi}^0}_{L3} &= B^{(l_k)}_{R\alpha a} D^{(x)}_{Lab} B^{(l_m)*}_{R\alpha b}, & \iota^{x,\tilde{\chi}^0}_{L3} &= B^{(l_k)}_{L\alpha a} B^{(l_m)*}_{R\beta a}, \\
\kappa^{x,\tilde{\chi}^0}_{L4} &= B^{(l_k)}_{L\alpha a} D^{(x)}_{Rab} B^{(l_m)*}_{L\alpha b}, & & \\
\kappa^{x,\tilde{\chi}^0}_{L5} &= B^{(l_k)}_{R\alpha a} D^{(x)}_{Rab} B^{(l_m)*}_{R\alpha b}, & & \\
\kappa^{x,\tilde{\chi}^0}_{L6} &= B^{(l_k)}_{L\alpha a} D^{(x)}_{Lab} B^{(l_m)*}_{L\alpha b}, & & \\
\kappa^{x,\tilde{\chi}^0}_{L7} &= B^{(l_k)}_{L\alpha a} D^{(x)}_{Lab} B^{(l_m)*}_{R\alpha b}, & &
\end{aligned}$$

$$\Sigma^{\tilde{\chi}^0}_L(k^2) = -\frac{g^2}{16\pi^2} B_1(k^2, m^2_{\tilde{\chi}^0_a}, m^2_{\tilde{l}_\alpha}) B^{(l_k)}_{R\alpha a} B^{(l_m)*}_{R\alpha a}, \qquad m_{l_k}\Sigma^{\tilde{\chi}^0}_{Ls}(k^2) = \frac{g^2 m_{\tilde{\chi}^0_a}}{16\pi^2} B_0(k^2, m^2_{\tilde{\chi}^0_a}, m^2_{\tilde{l}_\alpha}) B^{(l_k)}_{L\alpha a} B^{(l_m)*}_{R\alpha a}. \tag{B2}$$

The coupling factors and self-energies appearing in the chargino contributions to the form factors $\kappa^{x,\tilde{X}^-}$, $\iota^{x,\tilde{X}^-}$, and $\Sigma^{\tilde{X}^-}$ can be obtained from the previous expressions for $\kappa^{x,\tilde{X}^0}$, $\iota^{x,\tilde{X}^0}$, and $\Sigma^{\tilde{X}^0}$ by making the replacements $m_{\tilde{X}^0_a} \to m_{\tilde{X}^-_i}$, $m_{\tilde{l}_\alpha} \to m_{\tilde{\nu}_\alpha}$, $B^{(l)} \to A^{(l)}$, $D^{(x)} \to W^{(x)}$, $a \to i$, and $b \to j$.

The form factors $F^{(i)}_{R,x}$, $i = 1, \ldots 8$ can be achieved from $F^{(i)}_{L,x}$, $i = 1, \ldots 8$ by exchanging the indices $L \leftrightarrow R$ everywhere.

[1] B. T. Cleveland *et al.*, Astrophys. J. **496**, 505 (1998); Kamiokande Collaboration, Y. Fukuda *et al.*, Phys. Rev. Lett. **77**, 1683 (1996); V. Gavrin, Nucl. Phys. B, Proc. Suppl. **91**, 36 (2001); W. Hampel *et al.*, Phys. Lett. B **447**, 127 (1999); M. Altmann *et al.* Phys. Lett. B **490**, 16 (2000); Super-Kamiokande Collaboration, Y. Fukuda *et al.*, Phys. Rev. Lett. **86**, 5651 (2001); **86**, 5656 (2001); SNO Collaboration, Q. R. Ahmad *et al.*, Phys. Rev. Lett. **87**, 071301 (2001); **89**, 011302 (2002); KamLAND Collaboration, K. Eguchi *et al.*, Phys. Rev. Lett. **90**, 021802 (2003).

[2] M. Gell-Mann, P. Ramond, and R. Slansky, in *Supergravity*, edited by P. van Nieuwenhuizen and D. Z. Freedman (North-Holland, Amsterdam, 1979), p. 315; Pierre Ramond, hep-ph/9809459; T. Yanagida, in *Proceedings of the Workshop on the Unified Theory and the Baryon Number in the Universe*, edited by O. Sawada and A. Sugamoto (KEK, Tsukuba, Japan, 1979), p. 95; S. L. Glashow, in *Proceedings of the 1979 Cargèse Summer Institute on Quarks and Leptons*, edited by M. Lévy, J.-L. Basdevant, D. Speiser, J. Weyers, R. Gastmans, and M. Jacob (Plenum, New York, 1980), pp. 687–713; R. N. Mohapatra and G. Senjanović, Phys. Rev. Lett. **44**, 912 (1980).

[3] Z. Maki, M. Nakagawa, and S. Sakata, Prog. Theor. Phys. **28**, 870 (1962); B. Pontecorvo, Zh. Eksp. Teor. Fiz. **33**, 549 (1957); **34**, 247 (1958).

[4] A. M. Curiel, M. J. Herrero, W. Hollik, F. Merz, and S. Penaranda, Phys. Rev. D **69**, 075009 (2004).

[5] J. Hisano, T. Moroi, K. Tobe, M. Yamaguchi, and T. Yanagida, Phys. Lett. B **357**, 579 (1995); J. Hisano, D. Nomura, and T. Yanagida, Phys. Lett. B **437**, 351 (1998); S. F. King and M. Oliveira, Phys. Rev. D **60**, 035003 (1999); J. Hisano and D. Nomura, Phys. Rev. D **59**, 116005 (1999); J. R. Ellis, M. E. Gomez, G. K. Leontaris, S. Lola, and D. V. Nanopoulos, Eur. Phys. J. C **14**, 319 (2000); J. Hisano and K. Tobe, Phys. Lett. B **510**, 197 (2001); M. Frank, Phys. Rev. D **64**, 053013 (2001); S. Baek, T. Goto, Y. Okada, and K.-i. Okumura, Phys. Rev. D **64**, 095001 (2001); T. Blazek and S. F. King, Phys. Lett. B **518**, 109 (2001); S. Lavignac, I. Masina, and C. A. Savoy, Phys. Lett. B **520**, 269 (2001); A. Kageyama, S. Kaneko, N. Shimoyama, and M. Tanimoto, Phys. Rev. D **65**, 096010 (2002); T. Blazek and S. F. King, Nucl. Phys. **B662**, 359 (2003); B. Dutta and R. N. Mohapatra, Phys. Rev. D **68**, 056006 (2003); J. I. Illana and M. Masip, Eur. Phys. J. C **35**, 365 (2004); K. Tobe, J. D. Wells, and T. Yanagida, Phys. Rev. D **69**, 035010 (2004); A. Masiero, S. Profumo, S. K. Vempati, and C. E. Yaguna, J. High Energy Phys. 03 (2004) 046; A. Masiero, S. K. Vempati, and O. Vives, New J. Phys. **6**, 202 (2004).

[6] J. A. Casas and A. Ibarra, Nucl. Phys. **B618**, 171 (2001).

[7] P. H. Chankowski, J. R. Ellis, S. Pokorski, M. Raidal, and K. Turzynski, Nucl. Phys. **B690**, 279 (2004).

[8] S. Pascoli, S. T. Petcov, and C. E. Yaguna, Phys. Lett. B **564**, 241 (2003).

[9] MEGA Collaboration, M. L. Brooks *et al.*, Phys. Rev. Lett. **83**, 1521 (1999).

[10] BELLE Collaboration, K. Abe *et al.*, Phys. Rev. Lett. **92**, 171802 (2004).

[11] CLEO Collaboration, T. E. Coan *et al.*, Phys. Rev. D **55**, 7291 (1997).

[12] A. Pilaftsis, Phys. Lett. B **285**, 68 (1992); J. G. Korner, A. Pilaftsis, and K. Schilcher, Phys. Rev. D **47**, 1080 (1993).

[13] A. Pilaftsis, Z. Phys. C **55**, 275 (1992).

[14] J. L. Diaz-Cruz and J. J. Toscano, Phys. Rev. D **62**, 116005 (2000).

[15] A. Brignole and A. Rossi, Phys. Lett. B **566**, 217 (2003); Nucl. Phys. **B701**, 3 (2004).

[16] W. Grimus and L. Lavoura, J. High Energy Phys. 11 (2000) 042.

[17] P. H. Chankowski and Z. Pluciennik, Phys. Lett. B **316**, 312 (1993); K. S. Babu, C. N. Leung, and J. Pantaleone, Phys. Lett. B **319**, 191 (1993); N. Haba, N. Okamura, and M. Sugiura, Prog. Theor. Phys. **103**, 367 (2000); N. Haba, Y. Matsui, N. Okamura, and M. Sugiura, Eur. Phys. J. C **10**, 677 (1999); J. A. Casas, J. R. Espinosa, A. Ibarra, and I. Navarro, Nucl. Phys. **B556**, 3 (1999); **B569**, 82 (2000); M. Carena, J. R. Ellis, S. Lola, and C. E. M. Wagner, Eur. Phys. J. C **12**, 507 (2000); N. Haba and N. Okamura, Eur. Phys. J. C **14**, 347 (2000).

[18] M. C. Gonzalez-Garcia and C. Pena-Garay, Phys. Rev. D **68**, 093003 (2003).

[19] W. Hollik, in *Precision Tests of the Standard Electroweak Model*, edited by P. Langacker (World Scientific, Singapore, 1995), pp. 37–116; Fortschr. Phys. **38**, 165 (1990).

[20] R. Mertig, M. Bohm, and A. Denner, Comput. Phys. Commun. **64**, 345 (1991); T. Hahn and C. Schappacher, Comput. Phys. Commun. **143**, 54 (2002); T. Hahn, Comput. Phys. Commun. **140**, 418 (2001); T. Hahn and M. Perez-Victoria, Comput. Phys. Commun. **118**, 153 (1999).

[21] A. Djouadi, J. Kalinowski, and M. Spira, Comput. Phys. Commun. **108**, 56 (1998).

[22] A. Djouadi, J. L. Kneur, and G. Moultaka, hep-ph/

0211331.

[23] Y. Grossman and H. E. Haber, Phys. Rev. Lett. **78**, 3438 (1997).

[24] J. Hisano, T. Moroi, K. Tobe, and M. Yamaguchi, Phys. Rev. D **53**, 2442 (1996).

[25] K. S. Babu and C. Kolda, Phys. Rev. Lett. **89**, 241802 (2002).

[26] *BABAR* Collaboration, B. Aubert *et al.*, Phys. Rev. Lett. **92**, 121801 (2004); Belle Collaboration, Y. Yusa *et al.*, Phys. Lett. B **589**, 103 (2004).

[27] T. Han and D. Marfatia, Phys. Rev. Lett. **86**, 1442 (2001); U. Cotti, L. Diaz-Cruz, C. Pagliarone, and E. Vataga, in *Proceedings of the APS/DPF/DPB Summer Study on the Future of Particle Physics (Snowmass 2001)*, edited by N. Graf, eConf C010630, P102 (2001); J. L. Diaz-Cruz, J. High Energy Phys. 05 (2003) 036; K. A. Assamagan, A. Deandrea, and P. A. Delsart, Phys. Rev. D **67**, 035001 (2003); J. L. Diaz-Cruz, R. Noriega-Papaqui, and A. Rosado, Phys. Rev. D **69**, 095002 (2004).

[28] M. Sher, Phys. Lett. B **487**, 151 (2000); S. Kanemura, K. Matsuda, T. Ota, T. Shindou, E. Takasugi, and K. Tsumura, Phys. Lett. B **599**, 83 (2004).

[29] J. F. Gunion and H. E. Haber, Nucl. Phys. **B272**, 1 (1986); **B402**, 567(E) (1993).